Validation of Pan-Arctic Soil Temperatures in Modern Reanalysis and Data Assimilation Systems

Tyler C. Herrington [1], Christopher G. Fletcher [1], and Heather Kropp [2]

[1]Department of Geography and Environmental Management, University of Waterloo, 200 University Ave., Waterloo, Ontario, Canada, N2L 3G1

[2]Environmental Studies Program, Hamilton College, 198 College Hill Road, Clinton, 13323, New York, U.S.A.

Correspondence: Christopher G. Fletcher (chris.fletcher@uwaterloo.ca)

Abstract. Reanalysis products provide spatially homogeneous coverage for a variety of climate variables in regions where observational data are limited. However, very little validation of reanalysis soil temperatures in the Arctic has been performed to date, because widespread in situ reference observations have historically been unavailable there. Here we validate pan-Arctic soil temperatures from eight reanalysis and land data assimilation system products, using a newly-assembled database of in situ data from diverse measurement networks across Eurasia and North America. We find that most products have soil temperatures that are biased cold by 2-7 K across the Arctic, and that biases and RMSE are generally largest in the cold season (months where the mean air temperature is $\leq$ -2° C. Monthly mean values from most products correlate well with in situ data (r > 0.9) in the warm season, but show lower correlations (r = 0.6 - 0.8) over the cold season. Similarly, the magnitude of monthly variability in soil temperatures is well captured in summer, but overestimated by 20% to 50% for several products in winter. The suggestion is that soil temperatures in reanalysis products are subject to much higher uncertainty when the soil is frozen and/or when the ground is snow-covered. We also validate the ensemble mean of all available products, and find that, when all seasons and metrics are considered, the ensemble mean generally outperforms any individual product in terms of its correlation and variability, while maintaining relatively low biases. As such, we recommend the ensemble mean soil temperature product for a wide range of applications, such as the validation of soil temperatures in climate models, and to inform models that require soil temperature inputs, such as hydrological models.

1 Introduction

Soil temperatures, both near the surface, and at depth, are an important control of many physical, hydrological, and land surface processes, as soils act as a reservoir for energy and moisture underground. They provide an important initial condition for numerical weather prediction, as energy and water fluxes from the land are important for convective processes (Dirmeyer et al., 2006; Kim and Wang, 2007; Siqueira et al., 2009). As soils react relatively slowly to variations in weather, soil temperature is also an important predictor of seasonal and mid-term weather forecasts (Xue et al., 2011). Soils over large portions of the Arctic are perennially frozen (permafrost soil). Roughly 800 gigatonnes of carbon (GtC) is estimated to be stored in permafrost soils across the Northern Hemisphere (Hugelius et al., 2014); about twice the amount of carbon currently residing in the atmosphere (Tarnocai et al., 2009). Continued warming, and thawing of permafrost soils, and related decomposition of

carbon could act as a potential positive feedback on warming, by releasing more methane (CH_4) and carbon dioxide (CO_2) into the atmosphere (Koven et al., 2011).

In situ based soil temperature monitoring networks using thermistor probes, particularly at high latitudes, are limited in terms of their spatial and temporal coverage (Yi et al., 2019), making it difficult to assess hemispheric scale changes in permafrost. Reanalysis products have been used in a variety of weather and climate applications to provide information on a regular spatial grid; particularly in regions where limited or no observational data is available (Koster et al., 2004; Zhang et al., 2008). Previous studies validating reanalysis soil temperature have primarily focused on the middle latitudes, such as across China (Yang and Zhang, 2018; Xu et al., 2019; Zhan et al., 2020), the Qinqhai-Tibetan Plateau (Hu et al., 2019; Qin et al., 2020; Wu et al., 2018), Europe (Albergel et al., 2015; Johannsen et al., 2019), and the continental United States (Albergel et al., 2015; Xia et al., 2013), with a couple of recent studies validating soil temperatures globally (Li et al., 2020b). Relative to in situ ground temperature probe networks, most reanalysis products are biased cold by about 2°C - 5°C, on average (Hu et al., 2019; Qin et al., 2020; Yang and Zhang, 2018). Ma et al. (2021) found that most reanalysis products show larger cold biases over polar regions than they do over tropical and temperature regions, while a recent study by Cao et al. (2020) found that ERA5-Land soil temperatures were biased warm over the Arctic, particularly in winter.

Several explanations have been suggested for the biases in reanalysis soil temperatures, including model parameterizations (Albergel et al., 2015; Cao et al., 2020; Chen et al., 2015; Wu et al., 2018; Xiao et al., 2013), air temperature biases (Cao et al., 2020; Hu et al., 2017), errors in topography and elevation, arising from the coarse resolution of reanalysis products (Yang and Zhang, 2018; Zhao et al., 2008; Ma et al., 2021), and errors in simulated snow cover and snow thermal insulation (Cao et al., 2020; Royer et al., 2021).

While soil temperature biases in individual reanalysis products may limit their utility, a consensus is emerging that multi-reanalysis ensemble, based on the same principle as ensemble weather prediction (World Meteorological Organization, 2012), are an effective way to increase the signal-to-noise ratio for many important geophysical variables. Ensemble mean datasets based on combinations of in situ, model, satellite and reanalysis data have been used to reduce biases in estimates of snow water equivalent (Mudryk et al., 2015), soil moisture (Dorigo et al., 2017; Gruber et al., 2019), precipitation (Beck et al., 2017, 2019), as well as for local scale permafrost simulations (Cao et al., 2019). Hu et al. (2019) suggest that a similar method could be used to reduce biases in reanalysis soil temperatures.

Reanalysis soil temperatures have been relatively well characterized over the middle latitudes. Studies validating Arctic soil temperatures in reanalysis products, however, have either focused on a singular product (Cao et al., 2020), or have only considered a limited spatial extent (Li et al., 2020b; Ma et al., 2021).

Here we perform a validation of pan-Arctic (and Boreal) soil temperatures from eight reanalysis and land data assimilation system (LDAS) products. The main objectives are to 1) validate the 8 reanalysis and LDAS soil temperature products in terms of their bias, RMSE, correlation and standard deviation, and 2) investigate whether an ensemble mean soil temperature product outperforms the individual reanalysis products.

2 Data

2.1 Reanalysis and LDAS Data

Table 1 and 2 outline the six reanalysis and two LDAS soil temperature products used in this study. For simplicity, the term "reanalysis" will hereafter be used to describe both reanalysis and LDAS products. A summary of each product follows below. Products were remapped onto the Global Land Data Assimilation System – Catchment Land Surface Model (GLDAS-CLSM) grid for comparison, using three different methods: nearest neighbour, bilinear interpolation, and first-order conservative remapping. The choice of remapping method did not affect the overall conclusions of the study, and the analysis is based on data remapped using the conservative remapping method, as it facilitated the use of the largest number of validation sites and grid cells.

The reanalysis products investigated span a wide range of horizontal resolutions, ranging between 0.1°, in the case of ERA5-Land, to 1.0° for both GLDAS products (Table 1). Most products (CFSR, ERA-Interim, ERA5, ERA5-Land, and GLDAS-Noah) simulate soil temperature across 4 vertical layers, while MERRA2 and GLDAS-CLSM include 6 vertical layers, and JRA-55 calculates soil temperature across a single layer. The topmost soil layer has the highest resolution (7 cm to 10 cm in most cases), while the bottom soil layer often averages soil properties over a metre or more (Table 2).

The Noah Land Surface Model (Noah-LSM) (Chen et al., 1996; Betts et al., 1997; Koren et al., 1999; Ek, 2003) is used by CFSR and GLDAS-Noah. CFSR uses the Noah-LSM in a fully coupled mode to obtain a first-guess land-atmosphere simulation, before operating in a semi-coupled mode with GLDAS to obtain information about the state of the land surface (Saha et al., 2010). GLDAS, however, is run in an offline mode, utilizing meteorological forcing from Princeton University between 1948 to 2000 (Sheffield et al., 2006), and a combination of model and observational data from 2000 - onwards (Rui et al., 2018).

ERA-Interim, ERA5 and ERA5-Land use versions of the Tiled ECMWF Scheme for Surface Exchanges over Land (TESSEL) land model (Viterbo, 1995; Viterbo and Betts, 1999). In the case of ERA-Interim, TESSEL is informed by empirical corrections from 2m (surface) air temperature and humidity (Dee et al., 2011). Meanwhile, ERA5 and ERA5-Land use an updated version of TESSEL, known as the Hydrology-Tiled ECMWF Scheme for Surface Exchanges over Land (HTESSEL) (Balsamo et al., 2009). In ERA5, a weak coupling exists between the land surface and atmosphere. It includes an advanced LDAS that incorporates information regarding the near-surface air temperature, relative humidity, as well as snow cover (de Rosnay et al., 2014), along with satellite estimates of soil moisture and soil temperature from the top 1 metre of soil (de Rosnay et al., 2013). ERA5-Land, unlike ERA5, does not directly assimilate observational data. Instead, the ERA5 meteorology (such as air temperature, humidity and atmospheric pressure) is used as forcing information for HTESSEL; allowing it to be run at higher resolutions (Muñoz-Sabater et al., 2021). It includes an improved parameterization of soil thermal conductivity allowing for it to account for ice content in frozen soil, improvements to soil water balance conservation, and the ability to capture rain-on-snow events (Muñoz-Sabater et al., 2021).

Both GLDAS-CLSM and MERRA2 utilize the the Catchment Land Surface Model (CLSM) (Ducharne et al., 2000; Koster et al., 2000). Though MERRA2 does not include a land surface analysis (Gelaro et al., 2017), CLSM is informed using an

Table 1. Summary of the 8 reanalysis and LDAS products, their equatorial resolution, land model, and relevant references.

Product	Data Period	Resolution	Land Model	References
CFSR	1979 - 2010	0.31° x 0.31°	Noah LSM	Saha et al. (2010)
CFSv2	2011 - Present	0.2° x 0.2°	Noah LSM	Saha et al. (2014)
ERA-Interim	1979 - Aug 2019	0.75° x 0.75°	TESSEL	Dee et al. (2011)
ERA5	1979 - Present	0.25° x 0.25°	HTESSEL	Hersbach et al. (2020)
ERA5-Land	1981 - Present	0.1° x 0.1°	HTESSEL	Muñoz-Sabater et al. (2021)
GLDAS-CLSM	1948 - Present	1.0° x 1.0°	Catchment LSM	Rodell et al. (2004)
GLDAS-Noah	1948 - Present	1.0° x 1.0°	Noah LSM	Rodell et al. (2004)
JRA55	1956 - Present	0.56° x 0.56°	Simple Biosphere Model	Harada et al. (2016) Kobayashi et al. (2015)
MERRA2	1980 - Present	0.5° x 0.625°	Catchment LSM	Gelaro et al. (2017)

Table 2. Summary of the 8 reanalysis and LDAS products and the number and depths of the soil layers included. *The JRA-55 Simple Biosphere Model contains up to three soil layers (whose depths vary depending on vegetation type), but the soil temperature is averaged over all layers to produce a singular value at each grid cell.

Product	Soil Layers	Soil Depths (in cm)
CFSR	4	0 - 10, 10 - 40, 40 - 100, 100 - 200
CFSv2	4	0 - 10, 10 - 40, 40 - 100, 100 - 200
ERA-Interim	4	0 - 7, 7 - 28, 28 - 100, 100 - 289
ERA5	4	0 - 7, 7 - 28, 28 - 100, 100 - 289
ERA5-Land	4	0 - 7, 7 - 28, 28 - 100, 100 - 289
GLDAS-CLSM	6	0 - 9.88, 9.88 - 29.4, 29.4 - 67.99, 67.99 - 144.25, 144.25 - 294.96, 294.96 - 1294.96
GLDAS-Noah	4	0 - 10, 10 - 40, 40 - 100, 100 - 200
JRA55	3*	temperature averaged over soil column
MERRA2	6	0 - 9.88, 9.88 - 29.4, 29.4 - 67.99, 67.99 - 144.25, 144.25 - 294.96, 294.96 - 1294.96

updated version of the Climate Prediction Center unified gauge-based analysis of global daily precipitation (CPCU) precipitation correction algorithm that originated in MERRA-Land (Chen et al., 2008; Xie et al., 2007). No corrections are available, however, for high latitude regions north of 62.5° N (Reichle et al., 2017). In the case of GLDAS-CLSM, CLSM is run in an offline mode, in a similar configuration to GLDAS-Noah. Finally, JRA-55 uses the Simple Biosphere Model (SiB) (Onogi et al., 2007; Sato et al., 1988; Sellers et al., 1986) in an offline mode, forced by atmospheric data and data from land surface analyses that incorporate microwave satellite retrievals of snow cover (Kobayashi et al., 2015).

2.2 Observational Data

Owing to the lack of dense soil temperature monitoring networks in the Arctic, most of the observed soil temperature record is characterized by sparse measurements spanning different time periods (Yi et al., 2019). Rather than limit our validation to a small geographic region in the permafrost zone, as several prior studies have done (Hu et al., 2019; Qin et al., 2020; Wu et al., 2018; Ma et al., 2021; Li et al., 2020b), we choose to combine data from a variety of sparse networks. Such an approach

has been used to validate soil temperature and permafrost performance in ERA5-Land (Cao et al., 2020), and allows for the examination of larger geographic regions, as well as for the inclusion of a more diverse set of vegetation types across the continent (Ma et al., 2021).

The study compiles a comprehensive set of in situ soil temperature measurements across the Eurasian and North American Arctic, from multiple diverse sparse networks. The dataset incorporates data from the Yukon Geological Survey (Yukon Geological Survey, 2021), the Northwest Territories (Cameron et al., 2019; Ensom et al., 2020; Gruber et al., 2019; Spence and Hedstrom, 2018a, b; Street et al., 2018), Roshydromet Network in Russia (Sherstiukov, 2012), Nordicana series D (Nordicana) (Allard et al., 2020; CEN, 2020a, g, b, c, d, e, f), Global Terrestrial Network for Permafrost (GTN-P) (GTN-P, 2018), and Kropp et al. (2020) - in an attempt to provide a representative estimate of soil temperature across the circumpolar Arctic. Our validation data also includes sites from outside regions typically underlain by permafrost, in order to facilitate a comparison of the performance of reanalysis soil temperatures at high latitudes with their performance in regions outside the permafrost zone. Thse include data from Kropp et al. (2020), Sherstiukov (2012), and GTN-P (2018), as well as data from the Manitoba Mesonet network (RoTimi Ojo and Manaigre, 2021), the Michigan Enviro-weather Network (Enviro-weather, 2022), the North Dakota Mesonet Network (North Dakota Mesonet Netowrk, 2022), and the Alberta Climate Information Service network (Alberta Agriculture, Forestry and Rural Economic Development, 2022). Data is also sourced from a peatland ecosystem in Metro Vancouver (Beck et al., 2017; Lee et al., 2021), several locations in central and Northern BC (Déry, 2017; Hernández-Henríquez et al., 2018; Morris et al., 2021), and two locations in southern Quebec (Arsenault et al., 2018; Fortier, 2020). This provides a unique baseline upon which to perform a hemispheric wide assessment of soil temperature in reanalysis and LDAS systems, and to the authors' knowledge, presents the most comprehensive analysis to date of soil temperatures across Canada and the Great Lakes basin.

2.3 Collocation of Station and reanalysis Data

In order to compare with data from reanalysis and LDAS products, temperatures were averaged across two depth bins: a near surface layer (0 cm to 30 cm), and soil temperatures at depth (30 cm to 300 cm). For each site, temperatures from all depths residing within a layer were averaged, producing an estimated layer averaged temperature for every time-step. In order to maximize the amount of observational data available, layer-averaged soil temperatures were calculated at each timestep with all available data. This tradeoff meant that layer averages often included a different number of depths at different timesteps, and as such, we needed to limit our analysis of soil temperature trends and variability to locations where layer averages had a consistent number of depths.

Many of the in situ (station) sites reported measurements at hourly or daily frequency, however we chose to perform the analysis at monthly time scales, in order to focus on processes controlling the seasonal cycle of soil temperatures. As such, we use monthly averages of soil temperatures for validation purposes. Outlier observations with anomalies greater than $\pm$ 3.5σ were removed before monthly averaging.

Since the station data often included days with missing observations, the sensitivity of the monthly averages to missing data was tested, by computing monthly averages in five ways: using all months with at least one valid day in a month, using all

months with at least 25, 50, and 75 percent valid data, and finally using all months with no missing data in a month. It was found that T_{soil} was not substantially impacted by the inclusion or exclusion of months containing missing data. In order to increase sample size, we therefore included all months with at least 50 percent valid data.

In order to be considered as a validation location, the grid cell was required to include soil temperature data for all eight reanalysis/LDAS products, and be collocated with at least one in situ station. Duplicate stations across datasets were excluded. In situ locations were only included if there was at least 2 years worth of in situ data, in order to properly assess the station's seasonal cycle. For grid cells containing multiple in situ stations, the value used in the comparison is a simple spatial average of the in situ stations in that grid cell on each calendar day.

Over Eurasia, grid cells contained a single in situ measurement location. In North America, however, a number of the grid cells contain two or more in situ stations. The near surface layer layer includes 380 validation grid cells (Figure 1, panel A), while at depth, there are 346 grid cells (not shown). A subset of stations with longer timeseries and a more complete data record - mostly in Eurasia, are used to calculate soil temperature trends and variability (Section 4.2). Stations included in the soil temperature trend and variability analysis are shown as circles of varying size and colour, while those excluded from the soil temperature trend and variability analysis are shown as an x (Figure 1, Panel A). The details of Figure 1 - Panel A will be described further in Section 4.2.

To calculate spatial averages, a simple average of (layer-averaged) soil temperatures from all stations within the bounds of a particular grid cell was calculated at each timestep, using all available stations. This meant that the number of stations included at each timestep wasn't always consistent, and the analysis of soil temperature trends and variability was limited to a subset of grid cells where the following conditions were met:

1. The timeseries included at least 10 years of data.
2. The number of stations included in the spatially averaged grid cell temperature was consistent over all timesteps.
3. The number of depths included in the layer averaged soil temperature of each contributing station remained consistent over all timesteps.

As a result, many of the North American grid cells were excluded from the soil temperature trends analysis (except for a subset of 20 grid cells), and the bulk of the analysis is based on grid cells from Eurasia (where grid cells often only contained a single station) (Figure 1, Panel A). Using a subset of North American grid cells that incorporate multiple stations in the spatial average, and include a consistent number of stations and depths in the timeseries, we quantify the variability in soil temperatures between stations within a grid cell, and across depths within a layer average. It was found that the median temperature range between stations within a grid cell was approximately 2.3° C, which was roughly two to seven times larger than the median temperature range across depths within the near surface layer of a station (Figure 1, Panel B), suggesting that temperature variability within a grid cell is substantially larger than variations in temperatures within the near surface layer of a particular station.

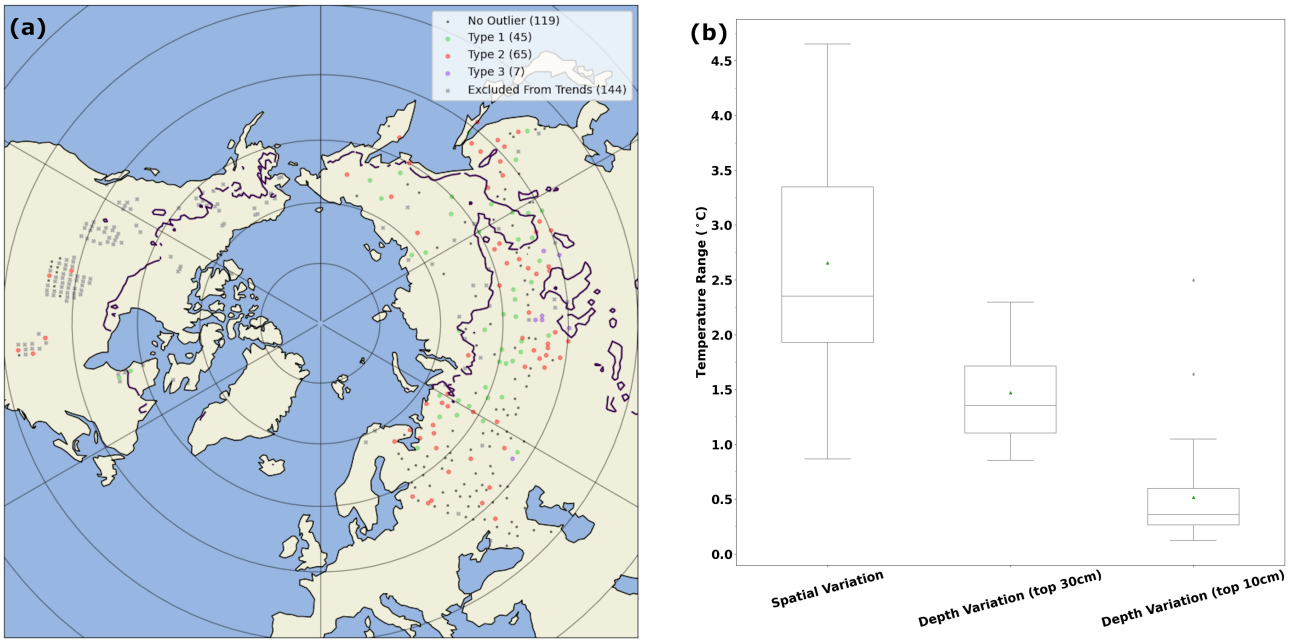

Figure 1. Panel A: location of the validation grid cells collocated with in situ stations in the near-surface layer. Grid cells excluded from the soil temperature trends analysis are shown as an "x". Type 1 refers to grid cells that where the ensemble mean simulates a winter minimum soil temperature that is too cold. Type 2 refers to grid cells where the ensemble mean simulates a summer maximum soil temperature that is too cold. Type 3 refers to grid cells where the ensemble mean underestimates the seasonal cycle of soil temperatures. The contour line encircles regions where the Obu et al. (2018) permafrost cover is at least 50 percent. Panel B: Impact of spatial variation and depth variation on the spread of soil temperatures in a grid cell. The mean is shown by a green triangle.

3 Methods

3.1 Validation Metrics

Reanalysis/LDAS and observational (station) soil temperature data were collocated with one another spatially and temporally. Grid-cell level soil temperatures from each product were compared against in situ soil temperatures using the following statistical metrics: bias (Eq. 1), root-mean-squared-error (RMSE) (Eq. 2), normalized standard deviation (SDV_{norm}) (Eq. 3 and Eq. 4), and the Pearson correlation (R) (Eq. 5). We also include an overall skill score for each model; a Thackeray et al. (2015) type formulation of the Taylor (2001) skill score (Eq. 6). Statistical metrics were calculated as follows:

$$Bias = \frac{1}{N}\sum_{n=1}^{N}(T_p - T_i) \tag{1}$$

$$RMSE = \sqrt{\frac{1}{N}\sum_{n=1}^{N}(T_p - T_i)^2} \tag{2}$$

$$SDV = \sqrt{\frac{\sum_{n=1}^{N}(x_n - \overline{x})^2}{N-1}} \tag{3}$$

$$SDV_{norm} = \frac{SDV_{T_p}}{SDV_{T_i}} \tag{4}$$

$$R = \frac{\frac{1}{N}\sum_{n=1}^{N}(T_p - \overline{T_p})(T_i - \overline{T_i})}{SDV_{T_p} SDV_{T_i}} \tag{5}$$

$$SS = \frac{2(1+R)}{(SDV_{norm} + \frac{1}{SDV_{norm}})^2} \tag{6}$$

Where T_p is the T_{soil} from the reanalysis product, and T_i is the T_{soil} of the in situ data. $\overline{T_p}$ and $\overline{T_i}$ refer to the mean T_{soil} of the reanalysis product and in situ data, respectively, while N is the number of monthly soil temperature values. SDV_{norm} refers to the normalized standard deviation, while SDV_{T_p} and SDV_{T_i} are the standard deviations of the reanalysis product soil temperatures and in situ soil temperatures, respectively. Finally, *x* refers to the T_{soil} (from a particular timestep in a dataset), $\overline{x}$ is the mean T_{soil} of the dataset, *R* is the Pearson correlation, and *SS* refers to the skill score.

Metrics were calculated separately for each individual grid cell, and then averaged to obtain regional values. Estimates for the permafrost zone and the zone with little to no permafrost were also calculated by averaging together metrics from grid cells falling within a particular zone. Skill scores were calculated separately for the near surface, and depth, while the "overall" skill score represents an average of the near surface and depth skill scores.

3.2 Binning of Datasets by Season and Permafrost

Datasets were binned into a cold season and warm season using the Berkeley Earth Surface Temperature (BEST) 2m air temperature (T_{air}) for each grid cell. Cold season months are those where $T_{air} \leq$ -2° C, while the warm season refers to months with T_{air} > -2° C, where T_{air} is the monthly mean air temperature. Sensitivity testing on the cold/warm season

revealed no substantive impact on our conclusions using a threshold of 0° C, -5° C, and -10° C. We also tested the impact of using a different temperature dataset to perform the binning; the ERA5 2m air temperature, which resulted in similar findings.

Permafrost zonation was estimated using the Obu et al. (2018) permafrost map, which employs a temperature at the top of the permafrost (TTOP) model based on a 2000-2016 climatology, driven by a combination of remotely sensed land surface temperatures, downscaled atmospheric data from ERA-Interim, and landcover information from The European Space Agency (ESA) Climate Change Initiative (CCI) (Obu et al., 2019). To maximize the sample size in each group, we merge the 'continuous' and 'extensive discontinuous' permafrost zones into a single category called the 'permafrost zone', and compare against the zone with 'little to no permafrost', which includes all regions with <50% permafrost cover.

3.3 Calculation of Ensemble Mean Product

The ensemble mean soil temperature product is a "blended" soil temperature product based on a simple average of soil temperatures from each of the individual soil temperature products (CFSR, ERA-Interim, ERA5, ERA5-Land, GLDAS-CLSM, GLDAS-Noah, JRA55 and MERRA2). Two soil temperature estimates: one of the "near-surface", and another of soil temperatures at depth are calculated for each timestep. The near-surface soil temperature is based on the average soil temperature of the top 2 soil layers from each product – representing an estimate of the average soil temperature in the top 30cm. The "deep" soil temperature estimate is based on an average of the soil temperatures from layers further down the soil column, down to a maximum depth of about 300cm. While the vertical discretization is coarser than that of the individual products, this approach allows the ensemble mean product to incorporate soil temperatures from products with different land models, whose vertical resolution is not constant.

All products were first re-gridded to the GLDAS-CLSM grid using a first-order conservative remapping technique (Jones, 1999). The near surface soil layers were calculated as a simple average of the top 2 soil layers in each reanalysis product (except for JRA-55 which only includes a single soil layer that represents the temperature averaged over the entire soil column). Soil temperatures at depth were calculated as a simple average of all layers whose bottom depth is within the top 300 cm of soil. For CFSR/CFSv2, ERA-Interim, ERA5 and ERA5-Land, this represented the third and fourth soil layers, while the third, fourth and fifth soil layers were included from MERRA2 and GLDAS-CLSM. For JRA55, we were again limited to the single averaged soil layer. Readers are referred to Table S1 for further information.

After the near surface and deep soil layer average temperatures were calculated for each product, the ensemble mean soil temperature, for each layer, was calculated as the unweighted arithmetic mean of the eight products for each month and for each grid cell.

4 Validation of reanalysis and LDAS Products

4.1 Extratropical Northern Hemisphere Mean

Most products show annual mean skill scores (purple) ranging between 0.8 and 0.95. In general, skill scores are higher near the surface where soil temperatures are more correlated with air temperatures (Figure 2). JRA55 is a noticeable outlier (skill score = 0.68), as it uses a simplified land model where the soil temperatures are averaged across the soil column. Thus its soil temperatures underestimate the seasonal cycle of observed soil temperatures in the near surface, and the timing of annual maximum and minimum soil temperatures is offset by roughly a month (as deep soil temperatures are slower to react to changes in air temperature or surface energy balance changes) (not shown).

For the most part, reanalyses show small to moderate negative (cold) biases in both seasons, though ERA5-Land exhibits a small positive (warm) bias in winter (Figure 2). JRA55 exhibits larger biases with respect to near surface soil temperatures, as it underestimates the annual range of near surface temperatures, whereas, at depth, biases are smaller, and the skill score is higher, reflective of the fact that its soil temperatures are more reflective of deeper soil layers. Generally speaking, most products show a maximum bias when soil temperatures are between -2° C to -10° C, and there is a tendency for biases to decrease or flip sign over the coldest temperatures. There is also a larger spread in bias over the coldest range of temperatures (Figure 3).

In addition, there is a larger range of temperatures displayed for a given observed soil temperature in the cold season (blue scatter) than in the warm season (red scatter) (Figure 4), suggesting a reduced agreement between reanalyses and observations in winter. For individual products, the variability in reanalysis soil temperature for a given observed soil temperature (as measured by their standard deviation) is generally greatest over frozen soil conditions (particularly temperatures below -20° C) - further evidence of the reduced agreement between product soil temperatures and observations. The spread in standard deviation between products (similar to their biases), is also largest over the coldest temperatures - providing evidence of increased disagreement between different reanalyses. JRA55 is an exception, as it shows a maximum standard deviation when soil temperatures are near freezing, and variance decreases thereafter (Figure 5) - likely due to the fact that it underestimates the coldest temperatures.

4.2 Temporal Variability

Strong seasonal differences exist in reanalysis performance - particularly near the surface, where skill scores are often 25% to 38% lower during the cold season than in warm season, and there is a noticeably larger spread (greater disagreement) between products. The skill at depth shows less seasonal variation, but is still noticeably lower during the cold season, with most products show a decline in skill of between 3% and 14%. The decline in cold season skill is mirrored by increases in near surface bias and RMSE for several products - particularly ERA-Interim, GLDAS-CLSM, and GLDAS-Noah whose biases are 4.1° C, 2.4° C and 1.7° C colder, respectively. Interestingly, biases for all products are somewhat larger in the warm season at depth, though seasonal differences are also generally smaller in the deeper soil layers (Figure 2).

JRA55 shows a 3.6° C positive (warm) bias during the cold season, and a 6.5° C negative (cold) bias in the warm season 2) - suggesting that the seasonal cycle in soil temperatures is too small. Meanwhile, ERA5-Land displays a small warm (positive) bias during the cold season; a feature not present in the warm season. This is suggestive that snow cover properties may be driving the winter warm bias in ERA5-Land (which will be discussed further in Section 6).

Similar seasonal variation is present in reanalysis soil temperature correlations (against station data), as most products show warm season correlations of greater than 0.95 near the surface 6). Meanwhile near surface cold season correlations are generally lower by approximately 0.2 to 0.3 (Figure 6) - which contributes to lower skill scores (Figure 2). The poor JRA55 correlation near the surface arises from its mismatched seasonal cycle.

Most products generally capture the observed soil temperature variance during the warm season, as normalized standard deviations are within 25% of the observed for all products. This is contrasted by the cold season, where several products overestimate soil temperature variability, contributing to a decline in product skill. Moreover, there is a larger spread in variance during the cold season - suggesting that there is less agreement between the products themselves (Figure 6). ERA5-Land's (blue) cold season skill is impacted by its underestimation of cold season soil temperature variability (which is roughly half of the observed variance), and arises in part because of its warm (positive) bias in winter (Figure 2). ERA-Interim (lime-green), GLDAS-Noah (black) and GLDAS-CLSM (grey) show unrealistically large soil temperature variability over the cold season (Figure 6), contributing to a substantial decline in their cold season skill (Figure 2).

4.3 Spatial Variability

Soil temperature performance over the permafrost zone is typically worse relative to the performance over the zone with little to no permafrost, while skill scores are generally reduced by 0.05 - 0.1, and by as much as 0.2 for ERA-Interim and ERA5-Land (Figure SRMSE are typically 2° C - 4° C larger over the permafrost zone (Figure S1 and Figure 7). The spread in standard deviation between products, at depth, is around 2.5 times larger over permafrost zone, relative to the zone with little to no permafrost (Figure S2), because of substantial differences in the variance of ERA5-Land, JRA55 and ERA-Interim. It is not clear whether these differences are due to the regions being colder, or due to structural issues with the land models, though this is beyond scope of paper. Interestingly, the differences in correlation and standard deviation between the permafrost zone, and the zone with little to no permafrost, in the near surface soil layers are less dramatic (Figure S2).

The ERA5-Land warm (positive) bias in the cold season is largest over permafrost regions (Figure S1) - particularly over Siberia and across North America (Figure S3). In the case of JRA55, however, the warm biases over the cold season are largest further south. In fact, over many grid cells in the permafrost zone, JRA55 exhibits a cold (negative) bias during the cold season (not shown).

Generally speaking, the skill is higher over Eurasia than over North America (Figure S4). The lower skill in North America arises in part due to the underestimation of seasonal cycle over many grid cells in the Yukon, and an overestimation of variability of cold season temperatures over much of the Great Lakes Region (Figure S5). CFSR, GLDAS-CLSM and JRA55 are an exception, however, as they greatly overestimate the cold season variability over much of western Eurasia (Figure S5), and consequently exhibit lower Eurasian skill scores. Product soil temperature correlations (with in situ soil temperatures) are also

lower by about 0.05 to 0.1 in both seasons over North America, relative to Eurasia (Figure S6), which further contributes to reduced skill over North America.

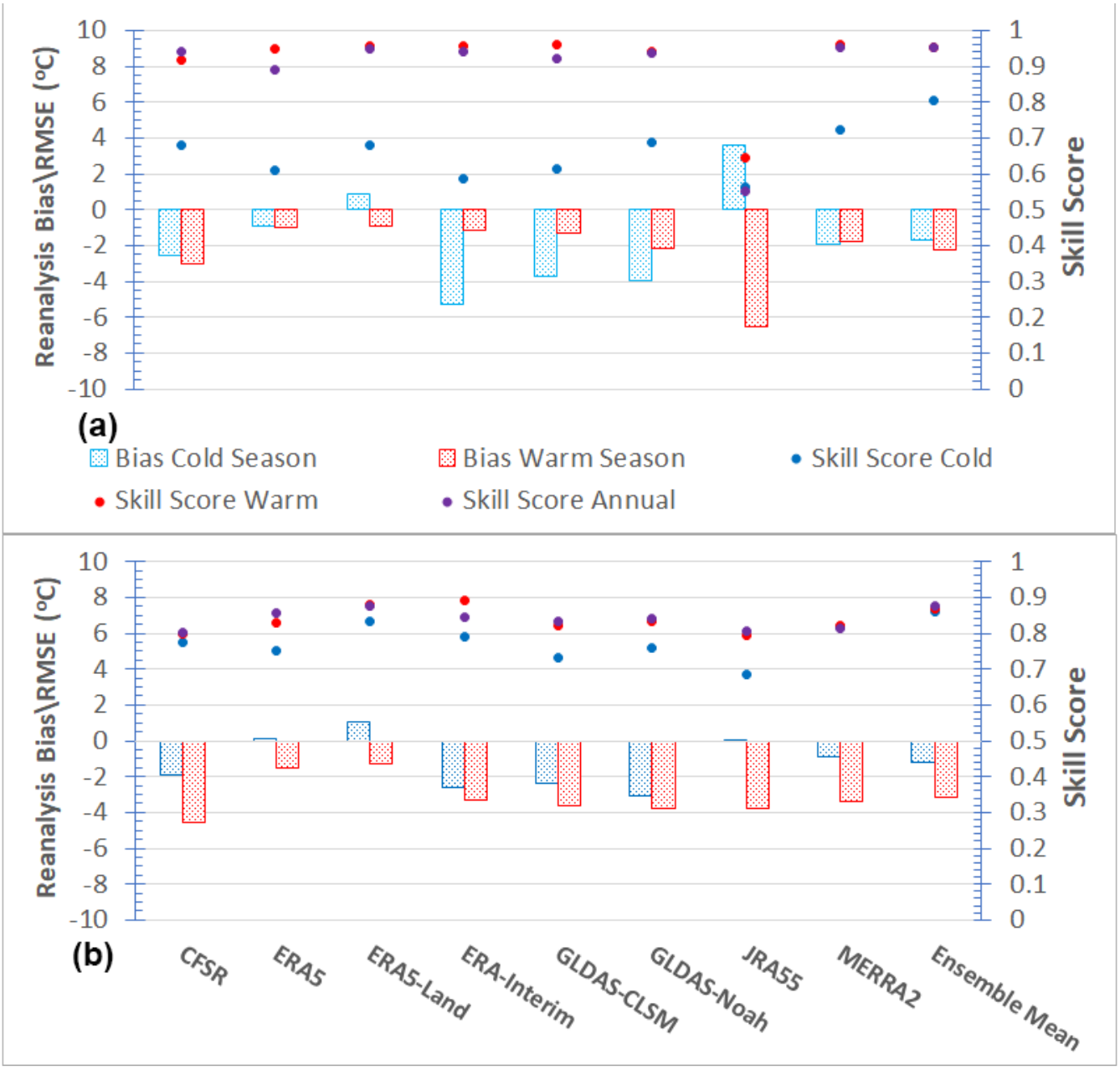

Figure 2. Bias (stippling) and skill scores (small circles) of each product the cold season (blue) ($\leq$ -2° C) and the warm season (red) (> -2° C) performance of reanalysis products. Panel A displays the bias and skill score for the near surface (0 cm to 30 cm) layer, while panel B displays the bias and skill score at depth (30 cm to 300 cm). The ensemble mean is shown beside for comparison.

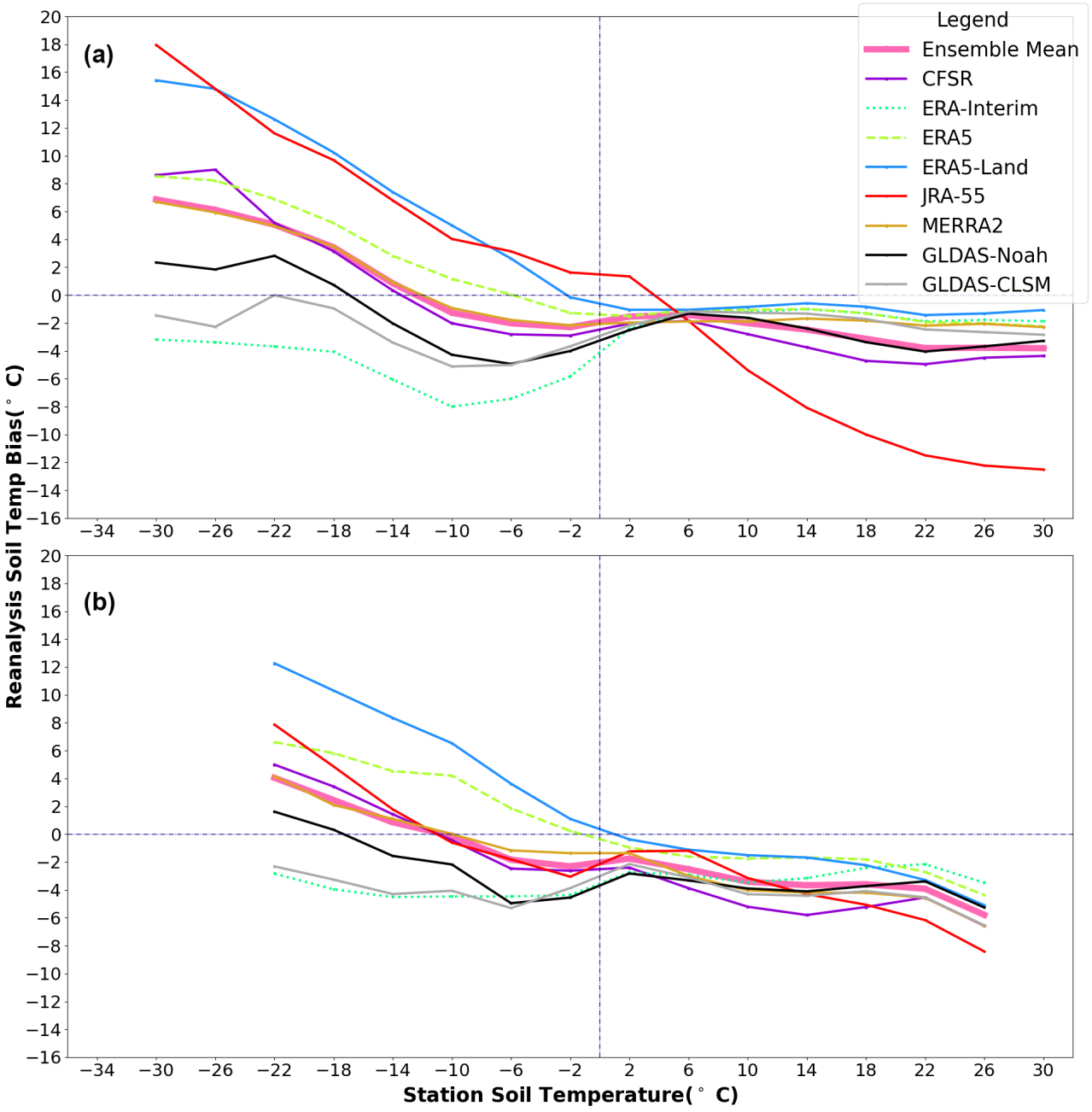

Figure 3. Reanalysis soil temperature bias as a function of station soil temperature for a) the near surface (0 cm to 30 cm) layer, and b) at depth (30 cm to 300 cm). Station temperatures are binned into 4° C intervals, beginning with the -32° C to -28° C bin, and ending with the 28° C to 32° C bin. The midpoint of each temperature bin is plotted along the x-axis.

5 Ensemble Mean Product

5.1 Validation

The ensemble mean soil temperature product produces a soil temperature dataset that shows closer agreement with observed soil temperatures than most/all individual products. The annual mean, ensemble mean skill score is higher than any individual product over the extratropical northern hemisphere (Figure 2). The bias of the ensemble mean soil temperature generally quite close in magnitude to the best performing products over both seasons depths (Figure 2). Moreover, the ensemble mean product (pink) displays a temporal variance within 20% of the observed variability over all depths. We find that the inclusion of a greater number of products in the ensemble mean yields greater reductions in bias and RMSE, and analogous improvements in correlation (Figure 8, panels A and B), though the incremental improvement in skill begins to saturate beyond four products (Figure 8.

The value of using the ensemble mean soil temperature is particularly noticeable in the cold season when individual products see a decline in skill, and a larger spread in performance. The near surface skill of the ensemble mean in the cold season is nearly 10% than the next best product (Figure 2). While many products fail to capture the cold season temperature variance, the variance of the ensemble mean product remains within 25% of the observed variability (Figure 2). In addition, the extratropical northern hemisphere mean cold season biases are close in magnitude to best performing product (Figure 2) over both depths, and its correlations are generally larger, by roughly 0.05, than the best performing product over both depths (Figure 6). Thus, the ensemble mean soil temperature dataset provides the best estimate of in situ temperatures for the broadest range of conditions.

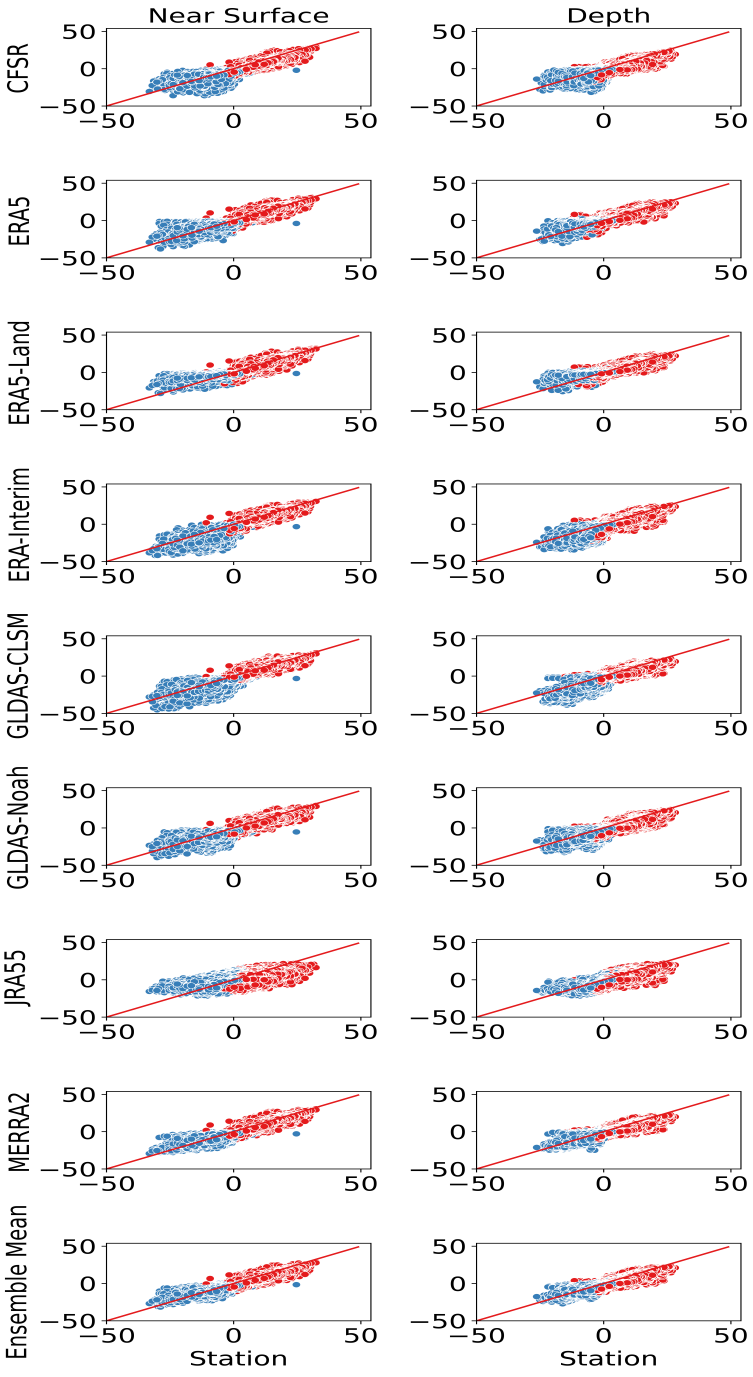

Figure 4. Scatterplot matrix of station and reanalysis soil temperatures. The left column is of soil temperatures in the near-surface (0 cm to 30 cm) layer, while the right column represents soil temperatures at depth (30 cm to 300 cm). Seasons are stratified by the BEST air temperature, with the cold season ($\leq$ -2° C) in blue and the warm season (>-2° C) in red.

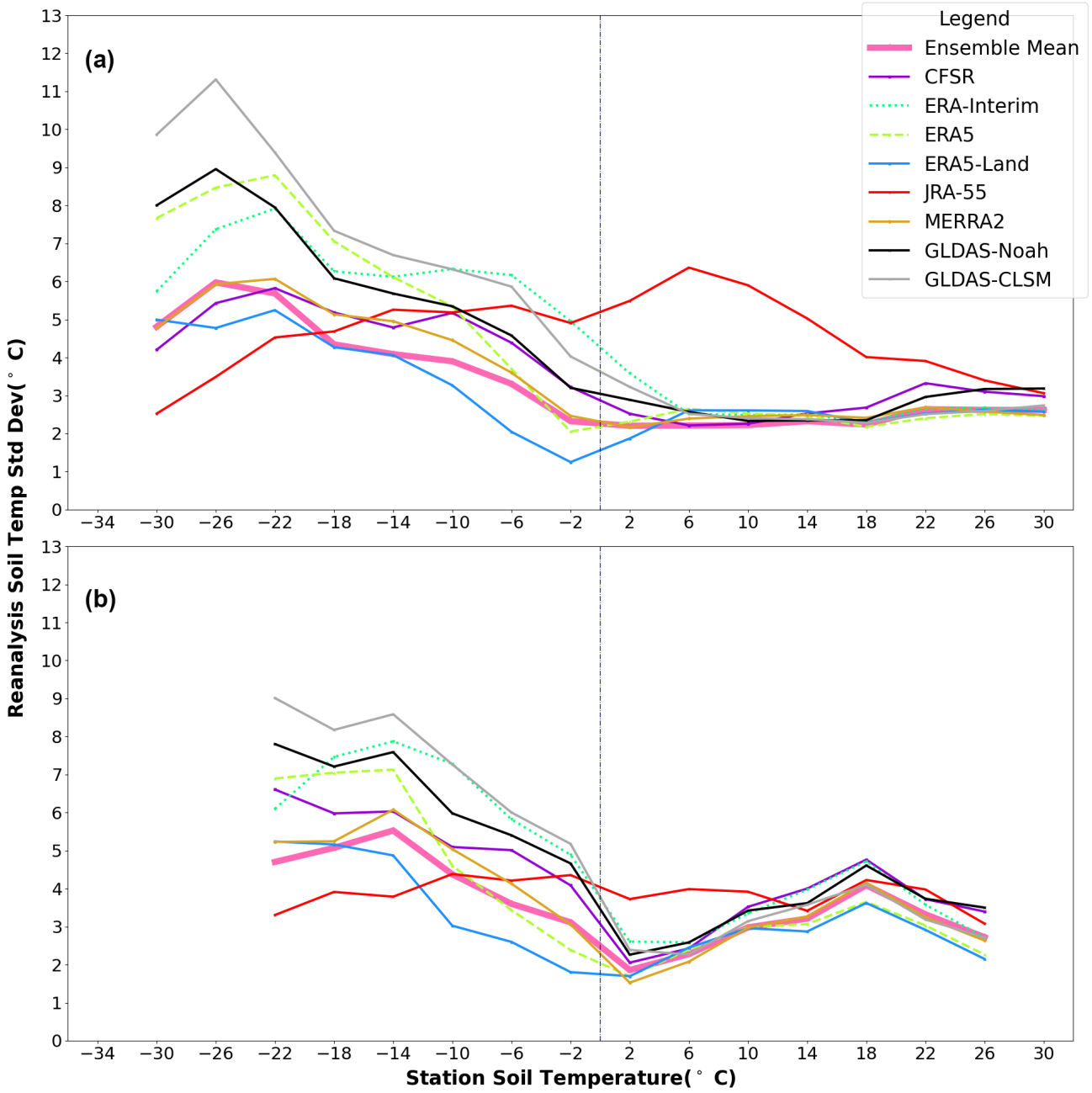

Figure 5. Reanalysis soil temperature standard deviation as a function of station soil temperature for a) the near surface (0 cm to 30 cm) layer, and b) at depth (30 cm to 300 cm). Station temperatures are binned into 4° C intervals, beginning with the -32° C to -28° C bin, and ending with the 28° C to 32° C bin. The midpoint of each temperature bin is plotted along the x-axis.

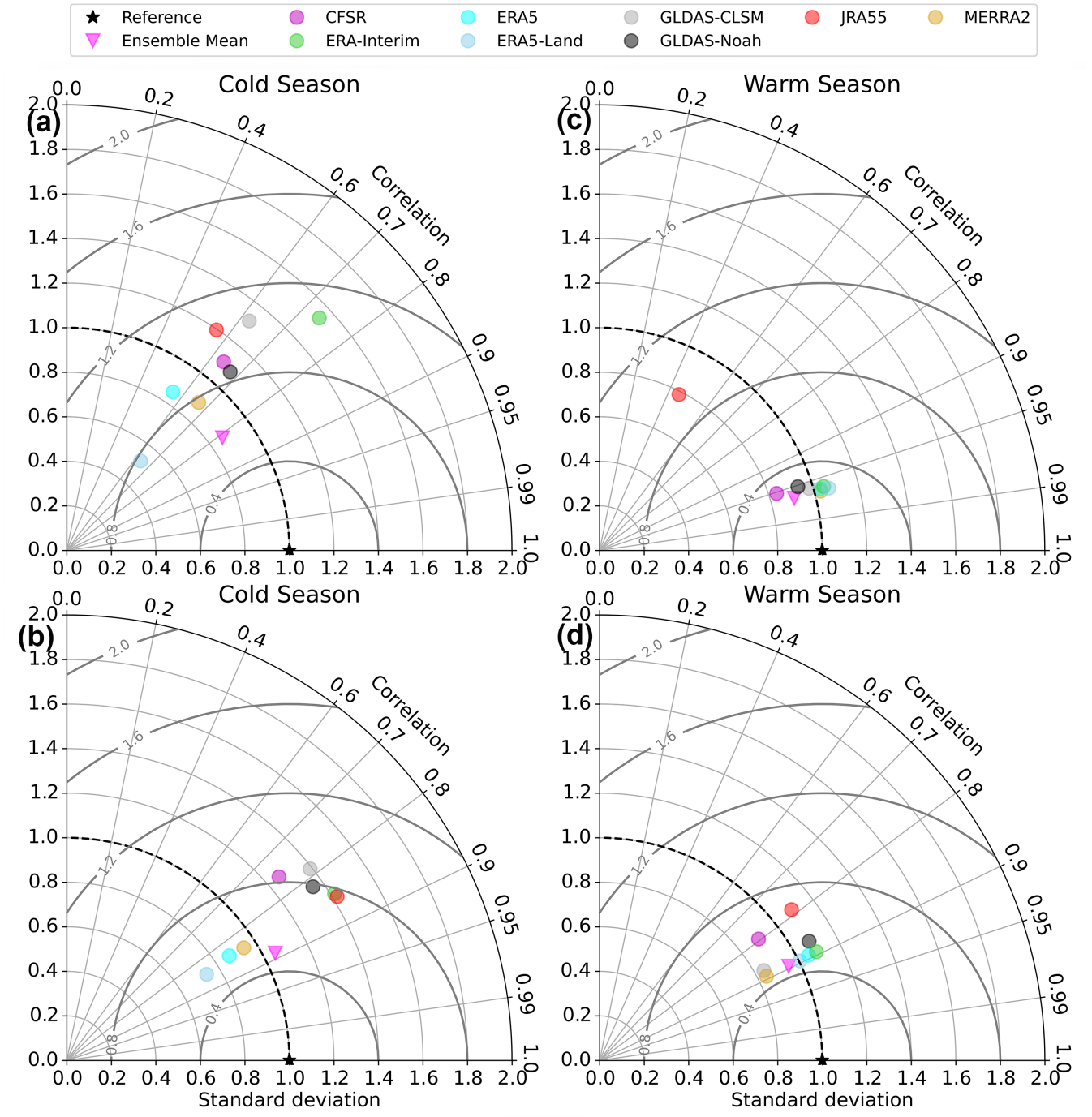

Figure 6. Taylor Diagram of the cold season ($\leq$ -2° C) and the warm season (> -2° C) performance of reanalysis products. Panels A and B refer to the cold season, while panels C and D refer to the warm season. The top panels (panels A and C) are for the near surface (0 cm to 30 cm) while the bottom panels (panels B and D) refer to soil temperatures at depth (30 cm to 300 cm). The concentric rings (solid grey lines) refer to the centralized root mean square error (CRMSE)

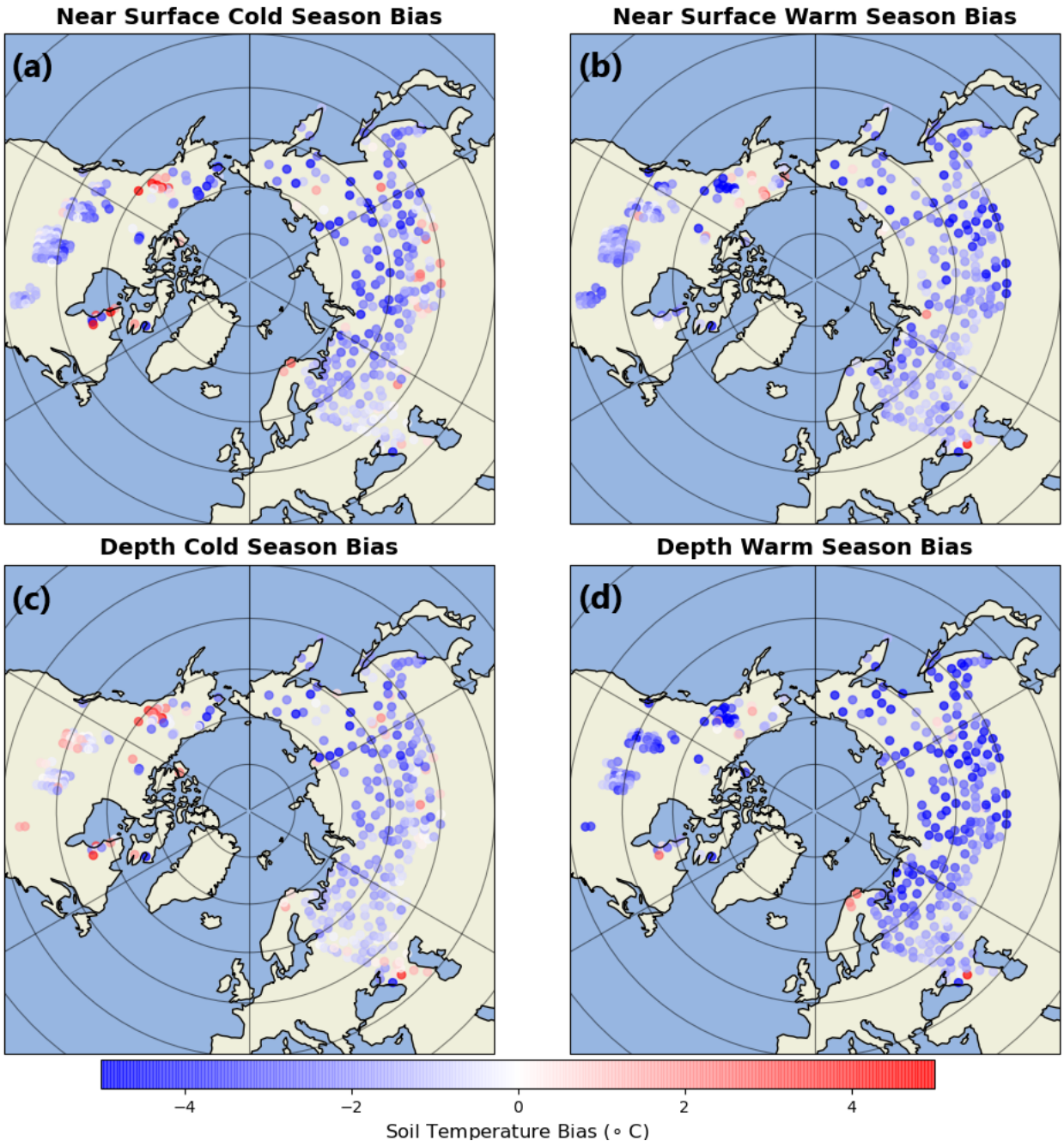

Figure 7. Spatial map of bias for the Ensemble Mean product. Values for the cold season are shown in the left hand panels, and those for the warm season are shown in the right hand panels. Panels A and B show the near surface bias, while biases at depth are shown in Panels C and D.

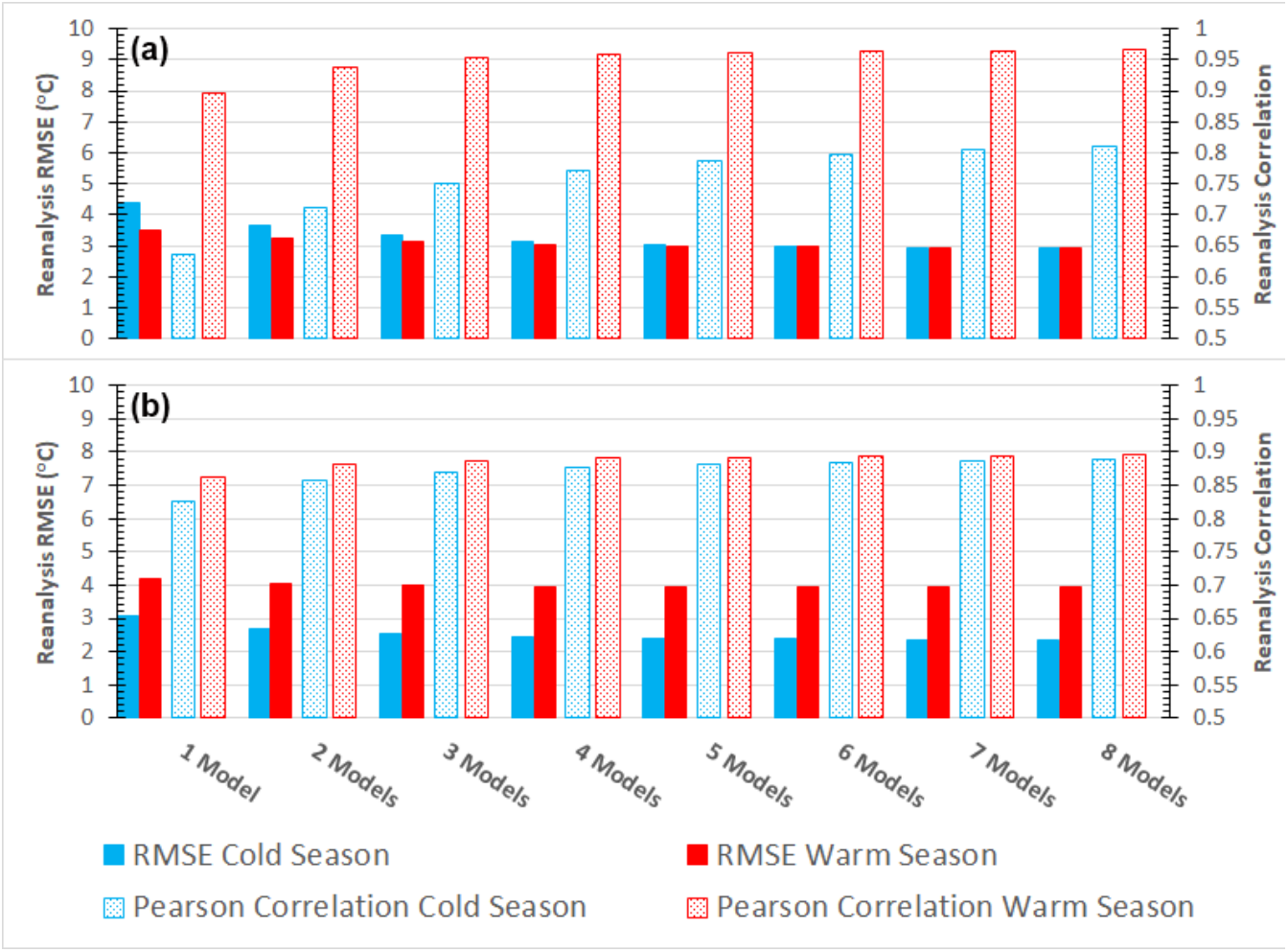

Figure 8. Root Mean Square Error (RMSE) (solid colour), and Pearson Correlation (stippling) for the cold season (blue) ($\leq$ -2° C) and the warm season (red) (> -2° C) averaged over all combinations of 1 model through to 8 model ensemble means. Panel A displays the RMSE and correlation for the near surface (0 cm to 30 cm) layer, while panel B displays the RMSE and correlation at depth (30 cm to 300 cm). Values are ordered based on cold season RMSE (from smallest to largest). Note that the y-axis scale is from -8° C to +10° C (rather than -10° C to +10° C).

5.2 Trends and Variability in Seasonal Extremes in the Ensemble Mean Product

We focus our analysis of variability and trends on the near surface data, as the spatial pattern of soil temperature trends near the surface and at depth show a pattern correlation of greater than 0.95 (not shown), and the conclusions regarding performance are generally similar. The authors highlight any major differences where applicable and readers are referred to Supplemental Figures A5 and A6 for further information.

The ensemble mean soil temperature dataset shows that most regions see small positive annual mean soil temperature trends of $\leq 1^{\circ}$ C decade^{-1}, with slightly larger trends in the Canadian Arctic Archipelago and in Siberia, for example. Portions of Western North America and Siberia exhibit slight cooling trends of $< 0.5^{\circ}$ C decade^{-1} (Figure 9, Panel A). Annual mean soil temperature trends in the Ensemble Mean over Eurasia show a moderate correlation of 0.5 with observations (Figure 9 Panel B). The ensemble mean generally correctly predicts both the magnitude and the sign of the station trend. There are several cases where the station shows a warming trend over North America, and the Ensemble Mean predicts a small cooling trend, however these trends are not statistically significant (Figure 9 Panel B). Figure S7 shows that the spatial pattern in soil temperature trends at depth is nearly identical (Panel A) - displaying a pattern correlation of 0.99. Panel B of Figure S7 highlights a similar performance of the Ensemble Mean product at depth - with most grid cells showing a small positive soil temperature trend, and a moderate correlation with in situ soil temperature trends of 0.45 (not shown).

Referring to Figure 1, Panel A, several different types of grid cells are denoted. The first group - Type 1 (45 occurrences) are typically located in regions within the permafrost zone; particularly in continental regions of Siberia. Type 1 grid cells are characterized by a strong cold bias in (underestimate) the winter minimum soil temperature (Figure **??**, Panel A). A second grouping of grid cells, which we refer to as Type 2 (65 occurrences), are generally located outside the permafrost zone, in grid cells that are further south, or in western Eurasia. Type 2 grid cells are defined as those which have a strong warm bias in (overestimate) the summer maximum temperature (Figure **??**, Panel B). A common feature of the third group, Type 3 (7 occurrences), is that they underestimate the observed seasonal cycle of soil temperatures (Figure **??**, Panel C). Often the situ station(s) located within Type 3 grid cells are located in areas devoid of vegetation, and it is likely that disagreements in the simulated vegetation cover in the contributing reanalysis products may partially account for the reduced seasonal cycle. Many grid cells in the Yukon, whose comprising stations are similarly located in areas devoid of vegetation, would also meet the criteria for a Type 3 outlier, as the ensemble mean normalized standard deviation (a measure of soil temperature variability) is substantially smaller than 1.0 in both seasons (Figure S7), though these grid cells were excluded as their timeseries were too short. If we examine all grid cells over North America, a fourth group can be identified: instances where the ensemble mean simulates a seasonal cycle of soil temperatures that is too large. This is evident in Figure S6, where a cluster of grid cells in the Great Lakes region show a normalized standard deviation much larger than 1.0. This is also true for a number of grid cells in western Eurasia.

As discussed in earlier sections, the mean soil temperatures in the ensemble mean product is generally biased cold (negative) over most grid cells in both seasons. For many grid cells, this cold bias also extends to both the winter minimum (Figure 11, Panel A) and the summer maximum (Figure 11, Panel B) soil temperature. As the previous paragraph, and Figure 11, Panels A

Table 3. Standard deviation (as a measure of spread between products) of the mean biases in winter minimum and summer maximum soil temperature, as a function of latitude and depth (from Figures 11 and S8, Panels C and D). Latitude bands are 10 degrees in width, such that the 40° N latitude band is an average between 40° N and 50° N, while the 60° N latitude band is an average between 60° N and 70° N, for example.

Latitude Band	Near Surface		Depth	
	Winter Minimum	Summer Maximum	Winter Minimum	Summer Maximum
40°N	2.60° C	2.30° C	1.21° C	1.47° C
50°N	2.90° C	2.47° C	1.56° C	1.56° C
60°N	3.73° C	2.73° C	2.70° C	1.68° C

and B show, however, there is a fair degree of variability in the behaviour of the ensemble mean seasonal extremes – making an assessment of the mean behaviour in seasonal extremes somewhat tricky. Therefore, in the following paragraphs, we will focus on the most robust findings.

Most products exhibit a cold bias over all latitude bands in both their zonal mean winter minimum (Figure 11, Panel C) and summer maximum temperature (Figure 11, Panel D). While the spread between products remains relatively consistent across latitudinal bands over summer, the spread between products increases at higher latitudes over winter (Table 3). Using the standard deviation as a measure of spread between product biases, the standard deviation in winter minimum bias increases from 2.60° C over the 40° N latitude band, to 3.73° C north of 60 ° N. This is in large part to substantially colder biases in ERA-Interim (green) at higher latitudes. Meanwhile the standard deviation in the mean summer maximum bias only sees small increases (from 2.30° C at 40° N, to 2.73° C at 60° N) (Table 3).

Winter warm (positive) biases in ERA5-Land (sky-blue) are most prevalent over higher latitudes. The ensemble mean (pink line) exhibits somewhat larger cold (negative) biases in winter minimum temperature in the highest latitude band (Figure 10, Panel C). Interestingly, ERA-Interim (green) shows similar biases to ERA5 (cyan) and ERA5-Land (sky-blue) in summer and is one of the best performing products. This is suggestive that ERA-Interim's degraded performance over winter could be related to snow cover.

The conclusions regarding variability in soil temperature extremes, at depth, are generally similar to those near the surface, though the spread between products is not quite as large as it is near the surface (Table 3). Both the winter minimum and summer maximum soil temperatures are biased cold at depth (Figure S8, Panels A and B), however the winter minimum soil temperature sees a larger spread at high latitudes (increasing from a standard deviation of 1.21° C at 40° N to 2.70° C at 60° N), while the spread in the summer maximum sees little variation with latitude (Table 3).

Figure S8 Panel B shows that there is a noticeably greater disagreement between the ensemble mean and in situ soil temperatures; especially over colder regions. It is also apparent that the latitudinally averaged biases in the summer maximum temperature (Figure S8, Panel C) are larger than their winter minimum counterparts (Figure S8, Panel D) - consistent with the findings that the extratropical mean bias in the warm season is larger than the bias in the cold season (Figure 2).

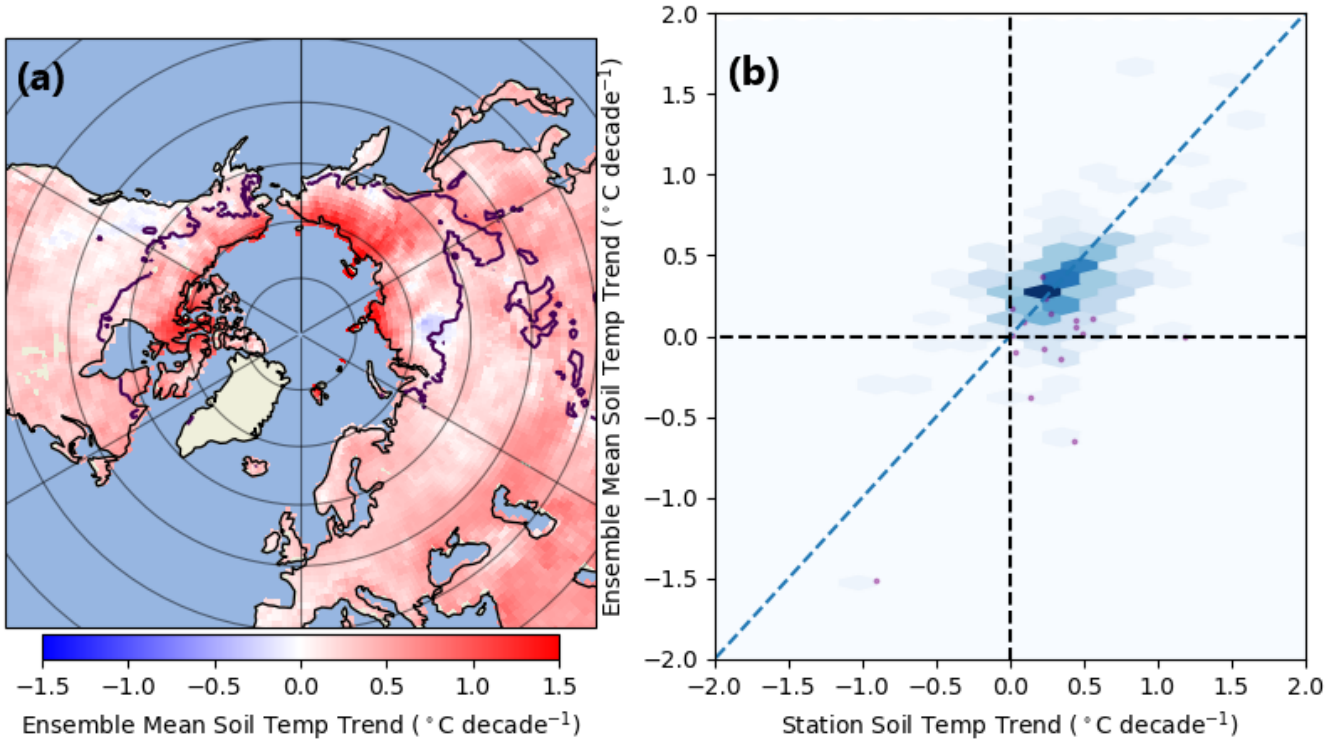

Figure 9. Panel A: 1981-2010 Ensemble Mean decadal soil temperature trends, with the locations of validation grid cells included in the trend analysis. Panel B: Relationship between Ensemble Mean and Station soil temperature trends (per decade). The red dots refer to North American grid cells. Note that the time periods over which the soil temperature trends are calculated in Panel B do not necessarily match those calculated in Panel A (as they are calculated over the time period that station data is available). The black line represents the boundary of the permafrost zone (regions with at least 50% permafrost cover).

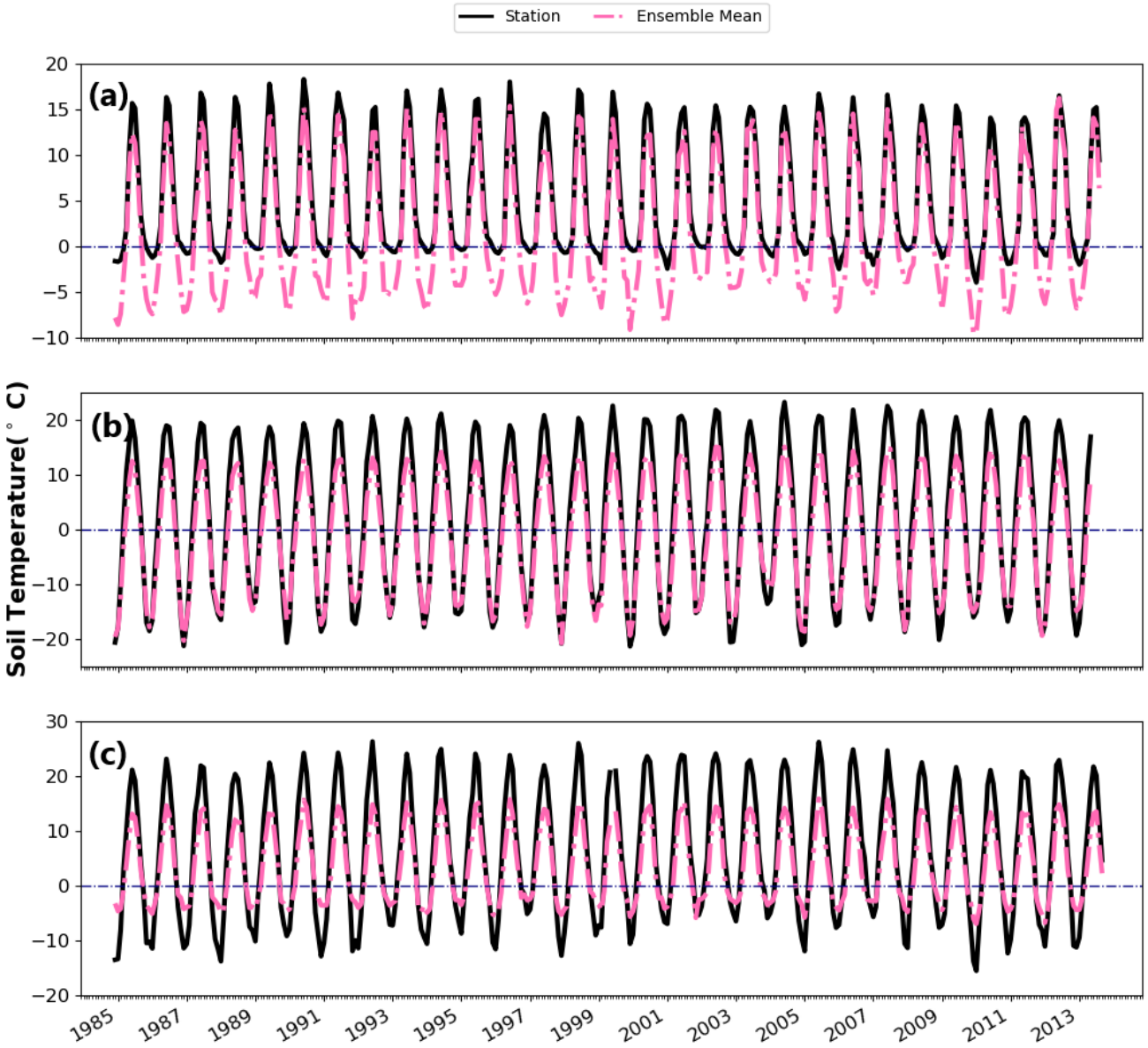

Figure 10. Timeseries from selected grid cells showing the ensemble mean (pink) and station (black) soil temperatures. Panel A: Timeseries where the ensemble mean simulates a winter minima that is too cold. Panel B: Timeseries where the ensemble mean simulates a summer maxima that is too cold. Panel C: Timeseries where the ensemble mean underestimates the seasonal cycle of soil temperatures.

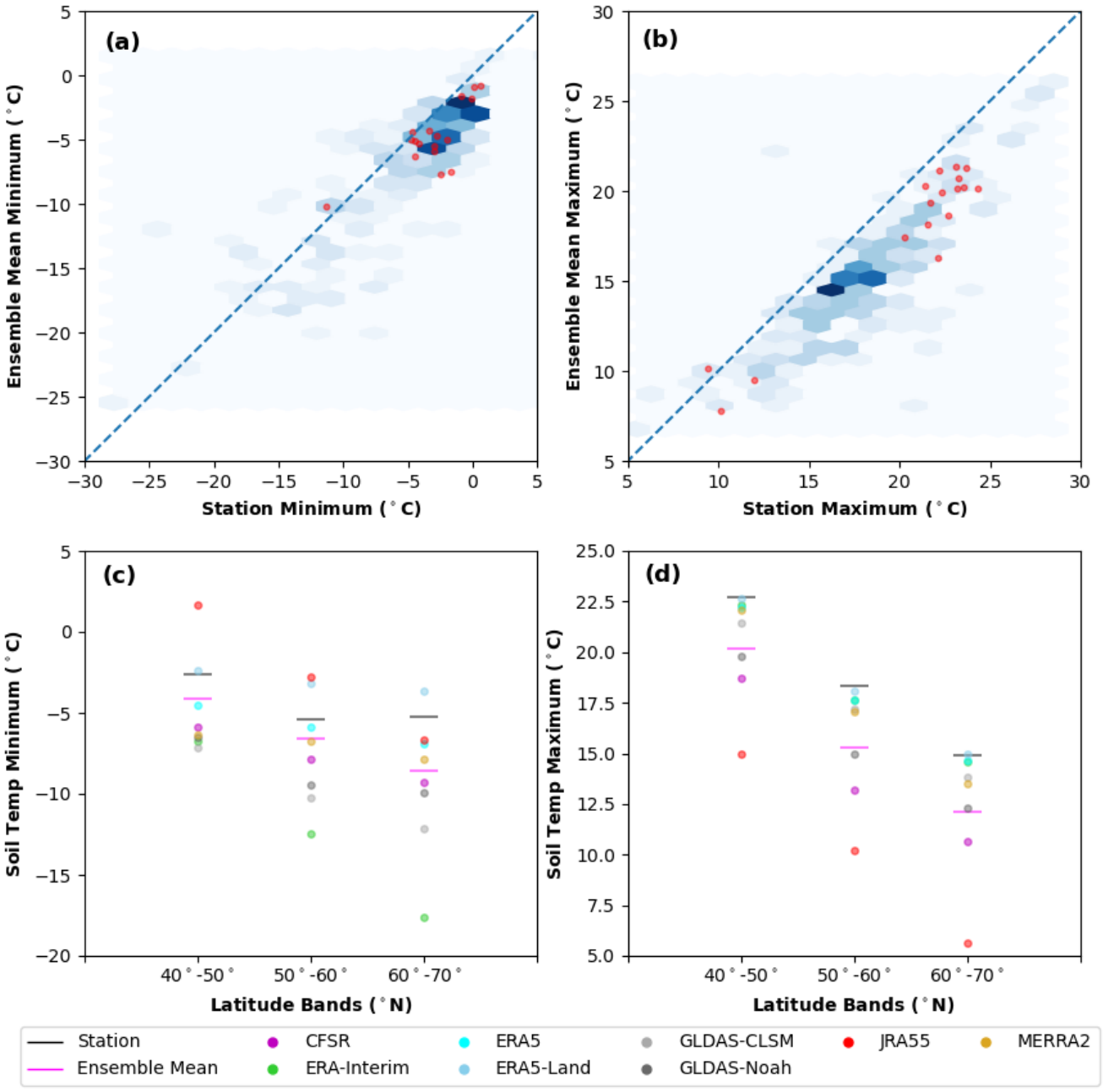

Figure 11. Performance of the near surface soil temperature variability in the Ensemble Mean. Panel A: Scatterplot of the station and ensemble mean winter minimum soil temperature. Panel B: Scatterplot of the station and ensemble mean summer maximum soil temperature. Panel C: latitudinal averages (from Eurasian grid cells) of near surface soil temperature winter minimum for the ensemble mean and contributing products. Panel D: latitudinal averages (from Eurasian grid cells) of near surface soil temperature summer maximum for the ensemble mean and contributing products.

6 Discussion and Conclusions

This study conducted a validation of pan-Arctic soil temperatures for eight reanalysis products, and validated a new ensemble mean pan-Arctic soil temperature dataset. The results are qualitatively similar to the findings of previous studies exploring reanalysis soil temperature performance in the extratropical northern hemisphere, which generally highlighted a cold bias in most products (Hu et al., 2019; Qin et al., 2020; Wu et al., 2018; Xu et al., 2019; Yang and Zhang, 2018; Zhan et al., 2020). Similar to (Li et al., 2021), we note greater biases in cold season soil temperatures, and our results qualitatively reflect the findings of Cao et al. (2020), who found that ERA5-Land exhibited warm soil temperature biases - particularly over higher latitudes.

The soil temperature trends reported here are slightly larger than those reported by Biskaborn et al. (2019), who found that permafrost soil temperatures generally warmed at a rate of 0.39° C $\pm$ 0.15° C decade^{-1}, however we report near surface soil temperature trends, whereas Biskaborn et al. (2019) used soil temperatures near the depth of zero amplitude to calculate soil temperature trends.

Other major differences here are that we develop an ensemble mean soil temperature product, and had a greater focus on higher latitude regions than most other studies. We also note a strong difference in seasonal performance. Relative to the warm season, the cold season is generally characterized by lower skill, larger near surface temperature biases, a larger spread in the reanalysis products' soil temperature variability and lower correlations with in situ soil temperatures. When all depths and seasons are considered, the ensemble mean product performs better than any individual product, exhibiting a consistently high skill, realistic soil temperature variability, and relatively small biases over all seasons.

Here we show an approximate estimate of the magnitude of soil temperature uncertainty associated with instrumental uncertainties, and those associated with structural differences and parameterizations in land models, using the standard deviation in soil temperature across time and as a function of station temperature. A complete quantitative assessment of the contributions of various sources of uncertainty is not possible using this dataset, as time-series did not have a consistent start or end date and consequently, the metrics are calculated using different climatologies across different grid cells. A more complete uncertainty analysis is beyond the scope here, but in the future could be achieved by limiting analysis to a subset of grid cells with consistent timeseries; for example by focusing on soil temperature networks such as the Michigan Enviro-weather Network, or the North Dakota Mesonet Network, or limiting the uncertainty analysis to a smaller portion of the permafrost region.

We find that the median spread in the spatially averaged soil temperature of stations in a grid cell is approximately 2.5° C (Figure 1, Panel B) – an order of magnitude smaller than the standard deviation of reanalysis soil temperatures for a given station soil temperature; particularly over frozen soils (Figure 5). For example, when soil temperatures are below –20 ° C, soil temperature standard deviations increase to near 10° C in several products. Reanalysis air temperatures maintain a relatively consistent standard deviation between 1.25° C to 1.75° C for most products, except over the coldest in situ temperatures (not shown). Unlike with soil temperature, the standard deviation of reanalysis two metre air temperature only increases modestly over the cold season; along with the spread in standard deviation between products (not shown). This would suggest that the largest degree of uncertainty in reanalysis soil temperatures over the Arctic is most likely contributed by differences in the

land models between products, rather than from uncertainties in observed soil temperatures, or from differences in product air temperatures.

6.1 Uncertainties Associated with Land Model Parameterizations and Structural Differences

Uncertainties in soil temperatures associated with structural differences and parameterizations in land models can be grouped into several categories. The first surrounds the simplified parameterizations controlling frozen soil processes. For example in the Noah LSM - utilized by CFSR and GLDAS-Noah, freeze-thaw processes are highly simplified, and unsuited for permafrost simulations (Hu et al., 2019) - and may have contributed to the relatively large soil temperature biases simulated in these products. Even the best performing products: ERA5 and ERA5-Land, are unsuited for simulation of permafrost soil temperatures, as they fail to simulate phase-dependent changes in soil thermal conductivity (Cao et al., 2020).

Yang et al. (2020) noted that larger soil temperature biases over the Qinghai-Tibetan Plateau in deeper soil layers were likely related to the fact that soil temperatures are less constrained by air temperature observations (and soil properties). This could also explain why soil temperature biases in the warm season are larger at depth than near the surface in this study. Moreover, the near surface soil layers tend to fall within the active layer (which undergoes seasonal freeze/thaw), while deeper soil layers are more likely to contain permafrost. Permafrost has a high degree of impermeability, which prevents soil water from infiltrating below the bottom of the active layer, and owing to latent heat considerations, leads to soil water freezing at the base of the active later (Zhao et al., 2000), however these processes are not well represented in reanalysis LSMs Yang et al. (2020); Hu et al. (2019).

LSMs such as the Simple Biosphere Model (used in JRA55), that use the force restore method to estimate soil temperature, are prone to overestimating diurnal soil temperature range (Gao et al., 2004; Kahan et al., 2006), as well as the seasonal cycle of soil temperatures (Luo et al., 2003). This is because they underestimate heat capacity, and overestimate temporal variation in ground heat flux compared to more complex land models (Hong and Kim, 2010). Moreover, the force restore method assumes a strong diurnal forcing from above, an assumption that is likely violated when snow cover is present (Tilley and Lynch, 1998; Slater et al., 2001), because snow cover leads to a decoupling of the surface forcing from the soil below. These factors may help explain why JRA55 is unable to simulate near surface soil temperatures as accurately as the other products explored in this study explicitly incorporate representations of soil heat flux between soil layers (Niu et al., 2011; Koster et al., 2000; van den Hurk et al., 2000; Balsamo et al., 2009), and hence they are able to simulate a dampening of seasonal variability of soil temperatures at depth (and greater variability near the surface).

Burke et al. (2020) note that differences in snow cover properties were important in explaining soil temperature biases of several Coupled Model Intercomparison Project 6 (CMIP6) models, and it is likely that differences in snow cover properties between the LSMs studied here could account for some of the observed spread - particularly in the cases of ERA-Interim, ERA5 and ERA5-Land, because during the warm season, these products have similar soil temperature biases, but their performance varies widely during the cold season (Figures 2 and 11), in large part because of snow density biases (Cao et al., 2020; Gao et al., 2022). In ERA-Interim, the large cold (negative) bias during the cold season is strongly related to the fact that it overestimates the observed snow density (Gao et al., 2022), and consequently also overestimates the thermal conductivity of the snow pack.

Conversely, snow density (and thermal conductivity) in ERA5-Land (and ERA5) are too low, and hence biases in snow density are a large contributing factor to the warm (positive) bias during the cold season (Cao et al., 2020). Snow was also cited as a major controlling factor in soil temperature biases in ECMWF's Integrated Forecast System, which also uses the HTESSEL land surface model (Albergel et al., 2015). In the case of the Noah LSM, which is included in CFSR/CFSv2 and GLDAS-Noah, Li et al. (2021) found that an overestimation of snow cover was a major contributor to larger soil temperature biases in winter over the Qinghai-Tibetan Plateau.

6.2 Impacts of Discontinuities in Reanalysis Timeseries

Discontinuities in the timeseries of reanalysis products may arise due to changes in data assimilation. This is particularly problematic when calculating soil temperature trends in reanalysis products, but will also influence correlation and variance on a Taylor diagram (such as Figure 6). Over the course of the nearly 40 year period explored in this study (1981 - 2018), CFSR and the two GLDAS products (GLDAS-CLSM, and GLDAS-Noah) see substantial changes in interannual variability in soil temperatures arising due to changes in data assimilation. GLDAS 2.0 (covering the period between 1948-1999) is forced using the Princeton meteorological forcing dataset, whereas GLDAS 2.1 (2000-onwards) uses a combination of modelled and observed data (Rodell et al., 2004). In a number of locations, there is a clear step-wise change in soil temperature variability around 2000 in both GLDAS products (not shown), coinciding with the shift from GLDAS 2.0 to GLDAS 2.1. CFSR sees a stepwise increase in soil temperature variability associated with the assimilation of Advanced TIROS Operational Vertical Sounder (ATOVS) radiance data beginning in 1998 (Saha et al., 2010; Xue et al., 2011). A decline in variability occurs around 2011, associated with the change from CFSR to CFSv2 (Saha et al., 2014). Unfortunately it is not trivial to remove the effects of temperature discontinuities in a timeseries; particularly when several products are being incorporated into an ensemble mean.

6.3 Uncertainties Associated with Scale Effects

Here we evaluated soil temperatures at a relatively coarse resolution of 1°. As such, it is difficult for reanalysis products to capture local scale variability in soil temperature. The sub-grid scale variability in soil temperatures calculated in Figure 1, Panel B is of a similar magnitude to those calculated by previous studies exploring sub-grid scale variability in cryospheric soil temperatures (Gubler et al., 2011; Morse et al., 2012; Gisnås et al., 2014), though is smaller than those reported by Cao et al. (2019). If the strict requirements surrounding consistency in the number of stations and depths are relaxed, allowing for stations in permafrost regions to be included, spatial variability in soil temperatures is larger than 10° C at times in a couple of high latitude grid cells (not shown) - similar to the findings of Cao et al. (2019).

Moreover, as many grid cells in Eurasia only included a single in situ station, there is a large chance that this single in situ station may not necessarily be reflective of conditions elsewhere in the grid cell (Gubler et al., 2011). When multiple in situ stations were available, we took the spatial mean of all stations, in an attempt to estimate the mean soil temperature over the grid cell.

6.4 Uncertainties Arising from Sampling Variability

As was described in Section 5.2, the presence of missing data created a challenge for calculating in situ soil temperature averages. While most grid cells in Eurasia had relatively consistent timeseries, and fewer issues with missing data, this was not the case over North America. Rather than limit our analysis to a small number of grid cells with little to no missing data (as we did for the calculation of soil temperature trends), we chose to make use of all available data at each timestep when calculating our validation metrics (bias, RMSE, standard deviation, correlation and skill score). Thus, the spatially averaged in situ soil temperature did not always contain a constant number of depths or grid cells at each timestep in many grid cells over North America.

From Figure 1, Panel B, it is apparent that the median variability of soil temperatures between stations within a grid cell (spatial variation) is roughly two to three times larger than the median variability of soil temperatures at different depths, in the top 30 cm, for a particular station (depth variation). Thus, it would appear that fluctuations in the number of stations comprising the spatially averaged soil temperature are responsible for a greater proportion of the uncertainty than fluctuations in the number of depths included. However it is also apparent that the uncertainties arising from variations in the number of grid cells included in a station average are smaller than the spread between reanalysis products; by a factor of two to three in the cold season.

6.5 Applications for the Ensemble Mean Product and Suggestions for Future Work

The ensemble mean data product provides gridded, monthly-averaged soil temperature estimates of near surface, and deeper soil temperatures at a 1° resolution. Therefore, it is most suitable to regional or hemispheric-scale analyses of soil temperature climatologies, or their seasonal cycle, or to explore recent trends in soil temperatures. The product could also be used to provide boundary conditions for models that require soil temperature inputs, such as hydrological models, and for the validation of model soil temperatures. While the ensemble mean product still exhibits substantial cold biases over permafrost regions, and therefore is likely unsuitable for permafrost modeling, the RMSE of the ensemble mean product outperforms the RMSE of the best performing product by 2° C, on average, and hence it may still provide some added value for estimation of high latitude soil temperatures relative to the individual products.

A robust ensemble mean can be computed with four products (Figure 8), which means a higher resolution ensemble mean data product could be created using a subset of higher resolution reanalysis products. For example, ERA-Interim, MERRA2, and CFSR have resolutions lower than 0.5 degrees. Using a similar blending methodology, we have been investigating the performance of a 0.31-degree product (using a smaller subset of products that provide data at higher spatial resolution). We have also performed similar analyses with a 0.05-degree soil temperature product, using interpolated soil temperatures from the Arctic System Reanalysis version 2 (ASR), ERA5-Land, and the Famine Early Warning Systems Network (FLDAS). The goal has been to assess the impact of spatial resolution on performance of the ensemble mean product. We are hoping to include these results in a follow-up paper. Future work should aim to investigate how differences in snow cover and snow density between

the reanalysis products may influence biases in the individual products. On a related note, future studies should emphasize how differences in the land model structure and parameterization may account for the spread in soil temperatures.

Data availability. GTN-P data (GTN-P, 2018) is available from The Global Terrestrial Network for Permafrost, while the Kropp et al. (2020) dataset is available from Heather Kropp's Arctic Data Center page. Russian Hydromet (Sherstiukov, 2012) data are available from RIHMI-WDC, while Nordicana data can be obtained from Nordicana D. CFSR (Saha et al., 2010), CFSv2 (Saha and Coauthors, 2012), ERA-Interim (European Centre for Medium-Range Weather Forecasts, 2012), ERA5 (European Centre for Medium-Range Weather Forecasts, 2019) and JRA-55 (Japan Meteorological Agency, 2013) data were obtained from the National Center for Atmospheric Research (NCAR)'s Research Data Archive (RDA). GLDAS-CLSM (Li et al., 2020a), GLDAS-Noah (Beaudoing et al., 2020), and MERRA2 (Global Modeling and Assimilation Office, 2015) were obtained from the Goddard Earth Sciences Data and Information Services Center (GES DISC), while ERA5-Land data (Muñoz-Sabater, 2019) was downloaded from the Copernicus Climate Change Service (C3S) Climate Data Store (CDS). The ensemble mean soil temperature dataset has been made available on the Arctic Data Center.

Author contributions. TH and CGF conceived of the study, TH gathered, and analyzed the data, and TH, CGF interpreted the data. HK provided in situ data to the study, and TH, and CGF wrote the manuscript, with contributions from HK.

Competing interests. The authors declare that they have no known conflicts - financial or personal, that could have appeared to influence this work.

Acknowledgements. This work was funded under a National Science and Engineering Research Council (NSERC) PGS-D scholarship. The authors would like to thank the two anonymous referees, as well as Dr. Hugh Brendan O'Neill and Dr. Andre Erler for their helpful comments.

References

Albergel, C., Dutra, E., Muñoz-Sabater, J., Haiden, T., Balsamo, G., Beljaars, A., Isaksen, L., de Rosnay, P., Sandu, I., and Wedi, N.: Soil Temperature at ECMWF: An Assessment Using Ground-Based Observations: Soil Temperature at ECMWF, Journal of Geophysical Research: Atmospheres, 120, 1361–1373, https://doi.org/10.1002/2014JD022505, 2015.

Alberta Agriculture, Forestry and Rural Economic Development: Current and Historical Alberta Weather Station Data., 2022.

Allard, M., Sarrazin, D., and Hérault, L.: Borehole and Near-Surface Ground Temperatures in Northeastern Canada, v. 1.5 (1988-2019). Nordicana D8, 2020.

Arsenault, D., Vézina, F., Sirois, L., Buffin-Bélanger, T., and Hétu, B.: Climate Station Data from Macpès Research Forest in the Rimouski Area, Quebec, Canada, v. 1.2 (2006-2017), 2018.

Balsamo, G., Beljaars, A., Scipal, K., Viterbo, P., van den Hurk, B., Hirschi, M., and Betts, A. K.: A Revised Hydrology for the ECMWF Model: Verification from Field Site to Terrestrial Water Storage and Impact in the Integrated Forecast System, Journal of Hydrometeorology, 10, 623 – 643, https://doi.org/10.1175/2008JHM1068.1, 2009.

Beaudoing, H., Rodell, M., and NASA/GSFC/HSL: GLDAS Noah Land Surface Model L4 Monthly 1.0 x 1.0 Degree V2.1, Greenbelt, Maryland, USA, 2020.

Beck, H. E., Vergopolan, N., Pan, M., Levizzani, V., van Dijk, A. I. J. M., Weedon, G. P., Brocca, L., Pappenberger, F., Huffman, G. J., and Wood, E. F.: Global-Scale Evaluation of 22 Precipitation Datasets Using Gauge Observations and Hydrological Modeling, Hydrology and Earth System Sciences, 21, 6201–6217, https://doi.org/10.5194/hess-21-6201-2017, 2017.

Beck, H. E., Pan, M., Roy, T., Weedon, G. P., Pappenberger, F., van Dijk, A. I. J. M., Huffman, G. J., Adler, R. F., and Wood, E. F.: Daily Evaluation of 26 Precipitation Datasets Using Stage-IV Gauge-Radar Data for the CONUS, Hydrology and Earth System Sciences, 23, 207–224, https://doi.org/10.5194/hess-23-207-2019, 2019.

Betts, A., Chen, F., Mitchell, K. E., and Janjić, Z. I.: Assessment of the Land Surface and Boundary Layer Models in Two Operational Versions of the NCEP Eta Model Using FIFE Data, Monthly Weather Review, 125, 2896–2916, 1997.

Biskaborn, B. K., Smith, S. L., Noetzli, J., Matthes, H., Vieira, G., Streletskiy, D. A., Schoeneich, P., Romanovsky, V. E., Lewkowicz, A. G., Abramov, A., Allard, M., Boike, J., Cable, W. L., Christiansen, H. H., Delaloye, R., Diekmann, B., Drozdov, D., Etzelmüller, B., Grosse, G., Guglielmin, M., Ingeman-Nielsen, T., Isaksen, K., Ishikawa, M., Johansson, M., Johannsson, H., Joo, A., Kaverin, D., Kholodov, A., Konstantinov, P., Kröger, T., Lambiel, C., Lanckman, J.-P., Luo, D., Malkova, G., Meiklejohn, I., Moskalenko, N., Oliva, M., Phillips, M., Ramos, M., Sannel, A. B. K., Sergeev, D., Seybold, C., Skryabin, P., Vasiliev, A., Wu, Q., Yoshikawa, K., Zheleznyak, M., and Lantuit, H.: Permafrost Is Warming at a Global Scale, Nature Communications, 10, 264, https://doi.org/10.1038/s41467-018-08240-4, 2019.

Burke, E. J., Zhang, Y., and Krinner, G.: Evaluating Permafrost Physics in the CMIP6 Models and Their Sensitivity to Climate Change, The Cryosphere, 14, 3155–3174, https://doi.org/10.5194/tc-2019-309, 2020.

Cameron, E., Lantz, T., O'Neill, H., Gill, H., Kokelj, S., and Burn, C.: Permafrost Ground Temperature Report: Ground Temperature Variability among Terrain Types in the Peel Plateau Region of the Northwest Territories (2011-2015), Tech. Rep. NWT 2017-009, Northwest Territories Geological Survey, Northwest Territories, Canada, 2019.

Cao, B., Quan, X., Brown, N., Stewart-Jones, E., and Gruber, S.: GlobSim (v1.0): Deriving Meteorological Time Series for Point Locations from Multiple Global Reanalyses, Geoscientific Model Development, 12, 4661–4679, https://doi.org/10.5194/gmd-12-4661-2019, 2019.

Cao, B., Gruber, S., Zheng, D., and Li, X.: The ERA5-Land Soil Temperature Bias in Permafrost Regions, The Cryosphere, 14, 2581–2595, https://doi.org/10.5194/tc-14-2581-2020, 2020.

CEN: Climate Station Data from Whapmagoostui-Kuujjuarapik Region in Nunavik, Quebec, Canada, v. 1.5 (1987-2019). Nordicana D4, 2020a.

CEN: Climate Station Data from the Sheldrake River Region in Nunavik, Quebec, Canada, v. 1.1 (1986-2019). Nordicana D61, 2020b.

CEN: Climate Station Data from the Clearwater Lake Region in Nunavik, Quebec, Canada, v. 1.1 (1986-2019). Nordicana D57, 2020c.

CEN: Climate Station Data from the Little Whale River Region in Nunavik, Quebec, Canada, v. 1.1 (1993-2019). Nordicana D58, 2020d.

CEN: Climate Station Data from the Biscarat River Region in Nunavik, Quebec, Canada, v. 1.0 (2005-2019). Nordicana D62., 2020e.

CEN: Climate Station Data from Northern Ellesmere Island in Nunavut, Canada, v. 1.7 (2002-2019). Nordicana D8, 2020f.

CEN: Environmental Data from Boniface River Region in Nunavik, Quebec, Canada, v. 1.3 (1988-2019). Nordicana D7, 2020g.

Chen, F., Mitchell, K., Schaake, Y., Xue, Y., Pan, H.-L., Koren, V., Duan, Q., Ek, M., and Betts, A.: Modeling of Land Surface Evaporation by Four Schemes and Comparison with FIFE Observations, Journal of Geophysical Research, 101, 7251–7268, 1996.

Chen, H., Nan, Z., Zhao, L., Ding, Y., Chen, J., and Pang, Q.: Noah Modelling of the Permafrost Distribution and Characteristics in the West Kunlun Area, Qinghai-Tibet Plateau, China: Noah Modelling of Permafrost, Permafrost and Periglacial Processes, 26, 160–174, https://doi.org/10.1002/ppp.1841, 2015.

Chen, M., Shi, W., Xie, P., Silva, V. B. S., Kousky, V. E., Wayne Higgins, R., and Janowiak, J. E.: Assessing objective techniques for gauge-based analyses of global daily precipitation, Journal of Geophysical Research: Atmospheres, 113, D04 110, https://doi.org/https://doi.org/10.1029/2007JD009132, 2008.

de Rosnay, P., Drusch, M., Vasiljevic, D., Balsamo, G., Albergel, C., and Isaksen, L.: A Simplified Extended Kalman Filter for the Global Operational Soil Moisture Analysis at ECMWF, Quarterly Journal of the Royal Meteorological Society, 139, 1199–1213, https://doi.org/10.1002/qj.2023, 2013.

de Rosnay, P., Balsamo, G., Albergel, C., Muñoz-Sabater, J., and Isaksen, L.: Initialisation of Land Surface Variables for Numerical Weather Prediction, Surveys in Geophysics, 35, 607–621, 2014.

Dee, D. P., Uppala, S. M., Simmons, A. J., Berrisford, P., Poli, P., Kobayashi, S., Andrae, U., Balmaseda, M. A., Balsamo, G., Bauer, P., Bechtold, P., Beljaars, A. C. M., van de Berg, L., Bidlot, J., Bormann, N., Delsol, C., Dragani, R., Fuentes, M., Geer, A. J., Haimberger, L., Healy, S. B., Hersbach, H., Hólm, E. V., Isaksen, L., Kållberg, P., Köhler, M., Matricardi, M., McNally, A. P., Monge-Sanz, B. M., Morcrette, J.-J., Park, B.-K., Peubey, C., de Rosnay, P., Tavolato, C., Thépaut, J.-N., and Vitart, F.: The ERA-Interim Reanalysis: Configuration and Performance of the Data Assimilation System, Quarterly Journal of the Royal Meteorological Society, 137, 553–597, https://doi.org/10.1002/qj.828, 2011.

Déry, S.: Cariboo Alpine Mesonet (CAMnet) Database, 2017.

Dirmeyer, P. A., Koster, R. D., and Guo, Z.: Do Global Models Properly Represent the Feedback between Land and Atmosphere?, Journal of Hydrometeorology, 7, 1177–1198, 2006.

Dorigo, W., Wagner, W., Albergel, C., Albrecht, F., Balsamo, G., Brocca, L., Chung, D., Ertl, M., Forkel, M., Gruber, A., Haas, E., Hamer, P. D., Hirschi, M., Ikonen, J., de Jeu, R., Kidd, R., Lahoz, W., Liu, Y. Y., Miralles, D., Mistelbauer, T., Nicolai-Shaw, N., Parinussa, R., Pratola, C., Reimer, C., van der Schalie, R., Seneviratne, S. I., Smolander, T., and Lecomte, P.: ESA CCI Soil Moisture for Improved Earth System Understanding: State-of-the Art and Future Directions, Remote Sensing of Environment, 203, 185–215, https://doi.org/10.1016/j.rse.2017.07.001, 2017.

Ducharne, A., Koster, R. D., Suarez, M. J., Stieglitz, M., and Kumar, P.: A Catchment-Based Approach to Modeling Land Surface Processes in a General Circulation Model: 2. Parameter Estimation and Model Demonstration, Journal of Geophysical Research: Atmospheres, 105, 24 823–24 838, https://doi.org/10.1029/2000JD900328, 2000.

Ek, M.: Implementation of Noah Land Surface Model Advances in the National Centers for Environmental Prediction Operational Mesoscale Eta Model, Journal of Geophysical Research, 108, https://doi.org/doi:10.1029/2002JD003296, 2003.

Ensom, T., Kokelj, S., and McHugh, K.: Permafrost Ground Temperature Report: Inuvik to Tuktoyaktuk Highway Stream Crossing and Alignment Sites, Northwest Territories, Tech. Rep. NWT Open Report 2019-004, Northwest Territories Geological Survey, Northwest Territories, Canada, 2020.

Enviro-weather: Enviro-Weather Aotmated Weather Station Network, 2022.

European Centre for Medium-Range Weather Forecasts: ERA-Interim Project, Monthly Means, 2012.

European Centre for Medium-Range Weather Forecasts: ERA5 Reanalysis (Monthly Mean 0.25 Degree Latitude-Longitude Grid), 2019.

Fortier, R.: Réseau Immatsiak de Surveillance Des Eaux Souterraines Dans La Région d'Umiujaq Au Nunavik, Québec, Canada, v. 1.4 (2012-2019)., 2020.

Gao, S., Li, Z., Zhang, P., Zeng, J., Chen, Q., Zhao, C., Liu, C., Wu, Z., and Qiao, H.: An Assessment of the Applicability of Three Reanalysis Snow Density Datasets Over China Using Ground Observations, IEEE Geoscience and Remote Sensing Letters, 19, 1–5, https://doi.org/10.1109/LGRS.2022.3202897, 2022.

Gao, Z., Chae, N., Kim, J., Hong, J., Choi, T., and Lee, H.: Modeling of Surface Energy Partitioning, Surface Temperature, and Soil Wetness in the Tibetan Prairie Using the Simple Biosphere Model 2 (SiB2): MODELING OF THE SURFACE PROCESSES, Journal of Geophysical Research: Atmospheres, 109, n/a–n/a, https://doi.org/10.1029/2003JD004089, 2004.

Gelaro, R., McCarty, W., Suárez, M. J., Todling, R., Molod, A., Takacs, L., Randles, C. A., Darmenov, A., Bosilovich, M. G., Reichle, R., Wargan, K., Coy, L., Cullather, R., Draper, C., Akella, S., Buchard, V., Conaty, A., da Silva, A. M., Gu, W., Kim, G.-K., Koster, R., Lucchesi, R., Merkova, D., Nielsen, J. E., Partyka, G., Pawson, S., Putman, W., Rienecker, M., Schubert, S. D., Sienkiewicz, M., and Zhao, B.: The Modern-Era Retrospective Analysis for Research and Applications, Version 2 (MERRA-2), Journal of Climate, 30, 5419–5454, https://doi.org/10.1175/JCLI-D-16-0758.1, 2017.

Gisnås, K., Westermann, S., Schuler, T. V., Litherland, T., Isaksen, K., Boike, J., and Etzelmüller, B.: A Statistical Approach to Represent Small-Scale Variability of Permafrost Temperatures Due to Snow Cover, The Cryosphere, 8, 2063–2074, https://doi.org/10.5194/tc-8-2063-2014, 2014.

Global Modeling and Assimilation Office: MERRA-2 tavg1_2d_lnd_Nx: 2d,1-Hourly,Time-Averaged,Single-Level,Assimilation,Land Surface Diagnostics V5.12.4, Greenbelt, MD, USA, 2015.

Gruber, S., Brown, N., Stewart-Jones, E., Karunaratne, K., Riddick, J., Peart, C., Subedi, R., and Kokelj, S. V.: Permafrost Ground Temperature Report: Ground Temperature and Site Characterisation Data from the Canadian Shield Tundra near Lac de Gras, Northwest Territories, Canada, Tech. Rep. NWT Open Report 2018-009, Northwest Territories Geological Survey, Northwest Territories, Canada, 2019.

GTN-P: GTN-P Global Mean Annual Ground Temperature Data for Permafrost near the Depth of Zero Annual Amplitude (2007-2016), https://doi.org/10.1594/PANGAEA.884711, 2018.

Gubler, S., Fiddes, J., Keller, M., and Gruber, S.: Scale-Dependent Measurement and Analysis of Ground Surface Temperature Variability in Alpine Terrain, The Cryosphere, 5, 431–443, https://doi.org/10.5194/tc-5-431-2011, 2011.

Harada, Y., Kamahori, H., Kobayashi, C., Endo, H., Kobayashi, S., Ota, Y., Onoda, H., Onogi, K., Miyaoka, K., and Takahashi, K.: The JRA-55 Reanalysis: Representation of Atmospheric Circulation and Climate Variability, Journal of the Meteorological Society of Japan. Ser. II, 94, 269–302, https://doi.org/10.2151/jmsj.2016-015, 2016.

Hernández-Henríquez, M. A., Sharma, A. R., Taylor, M., Thompson, H. D., and Déry, S. J.: The Cariboo Alpine Mesonet: Sub-Hourly Hydrometeorological Observations of British Columbia's Cariboo Mountains and Surrounding Area since 2006, Earth System Science Data, 10, 1655–1672, https://doi.org/https://ui.adsabs.harvard.edu/link_gateway/2018ESSD...10.1655H/doi:10.5194/essd-10-1655-2018, 2018.

Hersbach, H., Bell, B., Berrisford, P., Hirahara, S., Horányi, A., Muñoz-Sabater, J., Nicolas, J., Peubey, C., Radu, R., Schepers, D., Simmons, A., Soci, C., Abdalla, S., Abellan, X., Balsamo, G., Bechtold, P., Biavati, G., Bidlot, J., Bonavita, M., Chiara, G., Dahlgren, P., Dee, D., Diamantakis, M., Dragani, R., Flemming, J., Forbes, R., Fuentes, M., Geer, A., Haimberger, L., Healy, S., Hogan, R. J., Hólm, E., Janisková, M., Keeley, S., Laloyaux, P., Lopez, P., Lupu, C., Radnoti, G., Rosnay, P., Rozum, I., Vamborg, F., Villaume, S., and Thépaut, J.-N.: The ERA5 Global Reanalysis, Quarterly Journal of the Royal Meteorological Society, 146, 1999–2049, https://doi.org/10.1002/qj.3803, 2020.

Hong, J. and Kim, J.: Numerical Study of Surface Energy Partitioning on the Tibetan Plateau: Comparative Analysis of Two Biosphere Models, Biogeosciences, 7, 557–568, 2010.

Hu, G., Zhao, L., Wu, X., Li, R., Wu, T., Xie, C., Pang, Q., and Zou, D.: Comparison of the Thermal Conductivity Parameterizations for a Freeze-Thaw Algorithm with a Multi-Layered Soil in Permafrost Regions, CATENA, 156, 244–251, https://doi.org/10.1016/j.catena.2017.04.011, 2017.

Hu, G., Zhao, L., Li, R., Wu, X., Wu, T., Xie, C., Zhu, X., and Su, Y.: Variations in Soil Temperature from 1980 to 2015 in Permafrost Regions on the Qinghai-Tibetan Plateau Based on Observed and Reanalysis Products, Geoderma, 337, 893–905, https://doi.org/10.1016/j.geoderma.2018.10.044, 2019.

Hugelius, G., Strauss, J., Zubrzycki, S., Harden, J. W., Schuur, E. A. G., Grosse, G., Michaelson, G. J., Koven, C. D., O'Donnell, J. A., Elberling, B., Mishra, U., Camill, P., Yu, Z., Palmtag, J., and Kuhry, P.: Estimated Stocks of Circumpolar Permafrost Carbon with Quantified Uncertainty Ranges and Identified Data Gaps, Biogeosciences, 11, 6573–6593, 2014.

Japan Meteorological Agency: JRA-55: Japanese 55-Year Reanalysis, Monthly Means and Variances., 2013.

Johannsen, Ermida, Martins, Trigo, Nogueira, and Dutra: Cold Bias of ERA5 Summertime Daily Maximum Land Surface Temperature over Iberian Peninsula, Remote Sensing, 11, 2570, https://doi.org/10.3390/rs11212570, 2019.

Jones, P. W.: First- and Second-Order Conservative Remapping Schemes for Grids in Spherical Coordinates, Monthly Weather Review, 127, 2204–2210, https://doi.org/10.1175/1520-0493(1999)127<2204:FASOCR>2.0.CO;2, 1999.

Kahan, D. S., Xue, Y., and Allen, S. J.: The Impact of Vegetation and Soil Parameters in Simulations of Surface Energy and Water Balance in the Semi-Arid Sahel: A Case Study Using SEBEX and HAPEX-Sahel Data, Journal of Hydrology, 320, 238–259, https://doi.org/10.1016/j.jhydrol.2005.07.011, 2006.

Kim, Y. and Wang, G.: Impact of Vegetation Feedback on the Response of Precipitation to Antecedent Soil Moisture Anomalies over North America, Journal of Hydrometeorology, 8, 534–550, https://doi.org/10.1175/JHM612.1, 2007.

Kobayashi, S., Ota, Y., Harada, Y., Ebita, A., Moriya, M., Onoda, H., Onogi, K., Kamahori, H., Kobayashi, C., Endo, H., Miyaoka, K., and Takahashi, K.: The JRA-55 Reanalysis: General Specifications and Basic Characteristics, Journal of the Meteorological Society of Japan. Ser. II, 93, 5–48, https://doi.org/10.2151/jmsj.2015-001, 2015.

Koren, V., Schaake, J., Mitchell, K., and Chen, F.: A Parameterization of Snowpack and Frozen Ground Intended for NCEP Weather and Climate Models, Journal of Geophysical Research: Atmospheres, 104, 19 569–19 585, 1999.

Koster, R. D., Suarez, M. J., Ducharne, A., Stieglitz, M., and Kumar, P.: A Catchment-Based Approach to Modeling Land Surface Processes in a General Circulation Model: 1. Model Structure, Journal of Geophysical Research: Atmospheres, 105, 24 809–24 822, https://doi.org/10.1029/2000JD900327, 2000.

Koster, R. D., Suarez, M. J., Liu, P., Jambor, U., Berg, A., Kistler, M., Reichle, R., Rodell, M., and Famiglietti, J.: Realistic Initialization of Land Surface States: Impacts on Subseasonal Forecast Skill, Journal of Hydrometeorology, 5, 1049–1063, https://doi.org/10.1175/JHM-387.1, 2004.

Koven, C. D., Ringeval, B., Friedlingstein, P., Ciais, P., Cadule, P., Khvorostyanov, D., Krinner, G., and Tarnocai, C.: Permafrost Carbon-Climate Feedbacks Accelerate Global Warming, Proceedings of the National Academy of Sciences, 108, 14 769–14 774, https://doi.org/10.1073/pnas.1103910108, 2011.

Kropp, H., Loranty, M. M., Sannel, B., O'Donnell, J., and Blanc-Bates, E.: Synthesis of Soil-Air Temperature and Vegetation Measurements in the Pan-Arctic. 1990-2016. Arctic Data Center. Doi:10.18739/A2736M31X, 2020.

Lee, S.-C., Black, T. A., Nyberg, M., Merkens, M., Nesic, Z., Ng, D., and Knox, S. H.: Biophysical Impacts of Historical Disturbances, Restoration Strategies, and Vegetation Types in a Peatland Ecosystem, Journal of Geophysical Research: Biogeosciences, 126, https://doi.org/10.1029/2021JG006532, 2021.

Li, B., Beaudoing, H., Rodell, M., and NASA/GSFC/HSL: GLDAS Catchment Land Surface Model L4 Monthly 1.0 x 1.0 Degree V2.0, Greenbelt, Maryland, USA, 2020a.

Li, M., Wu, P., and Ma, Z.: Comprehensive Evaluation of Soil Moisture and Soil Temperature from Third-generation Atmospheric and Land Reanalysis Datasets, International Journal of Climatology, p. joc.6549, https://doi.org/10.1002/joc.6549, 2020b.

Li, X., Wu, T., Wu, X., Chen, J., Zhu, X., Hu, G., Li, R., Qiao, Y., Yang, C., Hao, J., Ni, J., and Ma, W.: Assessing the simulated soil hydrothermal regime of the active layer from the Noah-MP land surface model (v1.1) in the permafrost regions of the Qinghai–Tibet Plateau, Geoscientific Model Development, 14, 1753–1771, https://doi.org/10.5194/gmd-14-1753-2021, 2021.

Luo, L., Robock, A., Vinnikov, K. Y., Schlosser, C. A., Slater, A. G., Boone, A., Etchevers, P., Habets, F., Noilhan, J., Braden, H., Cox, P., de Rosnay, P., Dickinson, R. E., Dai, Y., Zeng, Q.-C., Duan, Q., Schaake, J., Henderson-Sellers, A., Gedney, N., Gusev, Y. M., Nasonova, O. N., Kim, J., Kowalczyk, E., Mitchell, K., Pitman, A. J., Shmakin, A. B., Smirnova, T. G., Wetzel, P., Xue, Y., and Yang, Z.-L.: Effects of Frozen Soil on Soil Temperature, Spring Infiltration, and Runoff: Results from the PILPS 2(d) Experiment at Valdai, Russia, Journal of Hydrometeorology, 4, 334–351, https://doi.org/10.1175/1525-7541(2003)4<334:EOFSOS>2.0.CO;2, 2003.

Ma, H., Zeng, J., Zhang, X., Fu, P., Zheng, D., Wigneron, J.-P., Chen, N., and Niyogi, D.: Evaluation of Six Satellite- and Model-Based Surface Soil Temperature Datasets Using Global Ground-Based Observations, Remote Sensing of Environment, 264, 112 605, https://doi.org/10.1016/j.rse.2021.112605, 2021.

Morris, J., Hernández-Henríquez, M., and Déry, S.: Cariboo Alpine Mesonet Meteorological Data, 2017-2021, 2021.

Morse, P., Burn, C., and Kokelj, S.: Influence of Snow on Near-Surface Ground Temperatures in Upland and Alluvial Environments of the Outer Mackenzie Delta, Northwest Territories., Canadian Journal of Earth Sciences, 49, 895–913, https://doi.org/10.1139/e2012-012, 2012.

Muñoz-Sabater, J.: ERA5-Land Monthly Averaged Data from 1981 to Present., 2019.

Muñoz-Sabater, J., Dutra, E., Agustí-Panareda, A., Albergel, C., Arduini, G., Balsamo, G., Boussetta, S., Choulga, M., Harrigan, S., Hersbach, H., Martens, B., Miralles, D. G., Piles, M., Rodríguez-Fernández, N. J., Zsoter, E., Buontempo, C., and Thépaut, J.-N.: ERA5-Land: A State-of-the-Art Global Reanalysis Dataset for Land Applications, Earth Syst. Sci. Data Discuss., https://doi.org/10.5194/essd-2021-82, 2021.

Mudryk, L. R., Derksen, C., Kushner, P. J., and Brown, R.: Characterization of Northern Hemisphere Snow Water Equivalent Datasets, 1981–2010, Journal of Climate, 28, 8037–8051, https://doi.org/10.1175/JCLI-D-15-0229.1, 2015.

Niu, G.-Y., Yang, Z.-L., Mitchell, K. E., Chen, F., Ek, M. B., Barlage, M., Kumar, A., Manning, K., Niyogi, D., Rosero, E., Tewari, M., and Xia, Y.: The community Noah land surface model with multiparameterization options (Noah-MP): 1. Model description and evaluation with local-scale measurements, Journal of Geophysical Research: Atmospheres, 116, https://doi.org/https://doi.org/10.1029/2010JD015139, 2011.

North Dakota Mesonet Netowrk: The North Dakota Mesonet Network, 2022.

Obu, J., Westermann, S., Kääb, A., and Bartsch, A.: Ground Temperature Map, 2000-2016, Northern Hemisphere Permafrost, https://doi.org/10.1594/PANGAEA.888600, 2018.

Obu, J., Westermann, S., Bartsch, A., Berdnikov, N., Christiansen, H. H., Dashtseren, A., Delaloye, R., Elberling, B., Etzelmüller, B., Kholodov, A., Khomutov, A., Kääb, A., Leibman, M. O., Lewkowicz, A. G., Panda, S. K., Romanovsky, V., Way, R. G., Westergaard-Nielsen, A., Wu, T., Yamkhin, J., and Zou, D.: Northern Hemisphere Permafrost Map Based on TTOP Modelling for 2000–2016 at 1 Km2 Scale, Earth-Science Reviews, 193, 299–316, https://doi.org/10.1016/j.earscirev.2019.04.023, 2019.

Onogi, K., Tsutsui, J., Koide, H., Sakamoto, M., Kobayashi, S., Hatsushika, H., Matsumoto, T., Yamazaki, N., Kamahori, H., Takahashi, K., Kadokura, S., Wada, K., Kato, K., Oyama, R., Ose, T., Mannoji, N., and Taira, R.: The JRA-25 Reanalysis, Journal of the Meteorological Society of Japan. Ser. II, 85, 369–432, https://doi.org/10.2151/jmsj.85.369, 2007.

Qin, Y., Liu, W., Guo, Z., and Xue, S.: Spatial and Temporal Variations in Soil Temperatures over the Qinghai–Tibet Plateau from 1980 to 2017 Based on Reanalysis Products, Theoretical and Applied Climatology, 140, 1055–1069, https://doi.org/10.1007/s00704-020-03149-9, 2020.

Reichle, R. H., Draper, C. S., Liu, Q., Girotto, M., Mahanama, S. P. P., Koster, R. D., and De Lannoy, G. J. M.: Assessment of MERRA-2 Land Surface Hydrology Estimates, Journal of Climate, 30, 2937–2960, https://doi.org/10.1175/JCLI-D-16-0720.1, 2017.

Rodell, M., Houser, P. R., Jambor, U., Gottschalck, J., Mitchell, K., Meng, C.-J., Arsenault, K., Cosgrove, B., Radakovich, J., Bosilovich, M., Entin, J. K., Walker, J. P., Lohmann, D., and Toll, D.: The Global Land Data Assimilation System, Bulletin of the American Meteorological Society, 85, 381–394, https://doi.org/10.1175/BAMS-85-3-381, 2004.

RoTimi Ojo, E. and Manaigre, L.: The Manitoba Agriculture Mesonet: Technical Overview, Bulletin of the American Meteorological Society, 102, E1786–E1804, https://doi.org/10.1175/BAMS-D-20-0306.1, 2021.

Royer, A., Picard, G., Vargel, C., Langlois, A., Gouttevin, I., and Dumont, M.: Improved Simulation of Arctic Circumpolar Land Area Snow Properties and Soil Temperatures, Frontiers in Earth Science, 9, 685 140, https://doi.org/10.3389/feart.2021.685140, 2021.

Rui, H., Beaudoing, H., and Loeser, C.: README Document for NASA GLDAS Version 2 Data Products, README Document, National Aeronautics and Space Administration, Maryland, USA, 2018.

Saha, S. and Coauthors: NCEP Climate Forecast System Version 2 (CFSv2) Monthly Products, 2012.

Saha, S., Moorthi, S., Pan, H.-L., Wu, X., Wang, J., Nadiga, S., Tripp, P., Kistler, R., Woollen, J., Behringer, D., Liu, H., Stokes, D., Grumbine, R., Gayno, G., Wang, J., Hou, Y.-T., Chuang, H.-y., Juang, H.-M. H., Sela, J., Iredell, M., Treadon, R., Kleist, D., Van Delst, P., Keyser, D., Derber, J., Ek, M., Meng, J., Wei, H., Yang, R., Lord, S., van den Dool, H., Kumar, A., Wang, W., Long, C., Chelliah, M., Xue, Y., Huang, B., Schemm, J.-K., Ebisuzaki, W., Lin, R., Xie, P., Chen, M., Zhou, S., Higgins, W., Zou, C.-Z., Liu, Q., Chen, Y., Han, Y., Cucurull, L., Reynolds, R. W., Rutledge, G., and Goldberg, M.: The NCEP Climate Forecast System Reanalysis, Bulletin of the American Meteorological Society, 91, 1015–1058, https://doi.org/10.1175/2010BAMS3001.1, 2010.

Saha, S., Moorthi, S., Wu, X., Wang, J., Nadiga, S., Tripp, P., Behringer, D., Hou, Y.-T., Chuang, H.-y., Iredell, M., Ek, M., Meng, J., Yang, R., Mendez, M. P., van den Dool, H., Zhang, Q., Wang, W., Chen, M., and Becker, E.: The NCEP Climate Forecast System Version 2, Journal of Climate, 27, 2185–2208, https://doi.org/10.1175/JCLI-D-12-00823.1, 2014.

Sato, N., Sellers, P., Randall, D., Schneider, E., Shukla, J., Kinter, III, J., Hou, Y.-T., and Albertazzi, E.: Effects of Implementing the Simple Biosphere Model in a General Circulation Model, Journal of the Atmospheric Sciences, 46, 2757–2782, https://doi.org/10.1175/1520-0469(1989)046<2757:EOITSB>2.0.CO;2, 1988.

Sellers, P. J., Mintz, Y., Sud, Y. C., and Dalcher, A.: A Simple Biosphere Model (SIB) for Use within General Circulation Models, Journal of the Atmospheric Sciences, 43, 505–531, https://doi.org/10.1175/1520-0469(1986)043<0505:ASBMFU>2.0.CO;2, 1986.

Sheffield, J., Goteti, G., and Wood, E.: Development of a 50-Year High-Resolution Global Dataset of Meteorological Forcings for Land Surface Modeling, Journal of Climate, 19, 3088–3111, 2006.

Sherstiukov, A.: Dataset of Daily Soil Temperature up to 320 Cm Depth Based on Meteorological Stations of Russian Federation [In Russian], Trudy VNIIGMI-MTsD, 176, 224–232, 2012.

Siqueira, M., Katul, G., and Porporato, A.: Soil Moisture Feedbacks on Convection Triggers: The Role of Soil–Plant Hydrodynamics, Journal of Hydrometeorology, 10, 96–112, https://doi.org/10.1175/2008JHM1027.1, 2009.

Slater, A. G., Schlosser, C. A., Desborough, C. E., Pitman, A. J., Henderson-Sellers, A., Robock, A., Vinnikov, K. Y., Entin, J., Mitchell, K., Chen, F., Boone, A., Etchevers, P., Habets, F., Noilhan, J., Braden, H., Cox, P. M., de Rosnay, P., Dickinson, R. E., Yang, Z.-L., Dai, Y.-J., Zeng, Q., Duan, Q., Koren, V., Schaake, S., Gedney, N., Gusev, Y. M., Nasonova, O. N., Kim, J., Kowalczyk, E. A., Shmakin, A. B., Smirnova, T. G., Verseghy, D., Wetzel, P., and Xue, Y.: The Representation of Snow in Land Surface Schemes: Results from PILPS 2(d), Journal of Hydrometeorology, 2, 7 – 25, https://doi.org/10.1175/1525-7541(2001)002<0007:TROSIL>2.0.CO;2, 2001.

Spence, C. and Hedstrom, N.: Baker Creek Research Catchment Hydrometeorological and Hydrological Data, 2018a.

Spence, C. and Hedstrom, N.: Hydrometeorological Data from Baker Creek Research Watershed, Northwest Territories, Canada, Earth Syst. Sci. Data, 10, 1753–1767, 2018b.

Street, L. E., Mielke, N., and Woodin, S. J.: Phosphorus Availability Determines the Response of Tundra Ecosystem Carbon Stocks to Nitrogen Enrichment, Ecosystems, 21, 1155–1167, https://doi.org/10.1007/s10021-017-0209-x, 2018.

Tarnocai, C., Canadell, J. G., Schuur, E. A. G., Kuhry, P., Mazhitova, G., and Zimov, S.: Soil Organic Carbon Pools in the Northern Circumpolar Permafrost Region: SOIL ORGANIC CARBON POOLS, Global Biogeochemical Cycles, 23, GB2023, https://doi.org/10.1029/2008GB003327, 2009.

Taylor, K. E.: Summarizing Multiple Aspects of Model Performance in a Single Diagram, Journal of Geophysical Research: Atmospheres, 106, 7183–7192, https://doi.org/10.1029/2000JD900719, 2001.

Thackeray, C. W., Fletcher, C. G., and Derksen, C.: Quantifying the Skill of CMIP5 Models in Simulating Seasonal Albedo and Snow Cover Evolution: CMIP5-SIMULATED ALBEDO AND SCF SKILL, Journal of Geophysical Research: Atmospheres, 120, 5831–5849, https://doi.org/10.1002/2015JD023325, 2015.

Tilley, J. S. and Lynch, A. H.: On the Applicability of Current Land Surface Schemes for Arctic Tundra: An Intercomparison Study, Journal of Geophysical Research, 103, 29 051–29 063, https://doi.org/doi:10.1029/1998JD200014, 1998.

van den Hurk, B., Viterbo, P., Beljaars, A., and Betts, A.: Offline validation of the ERA40 surface scheme, https://doi.org/10.21957/9aoaspz8, 2000.

Viterbo, P.: An Improved Land Surface Parametrization Scheme in the ECMWF Model and Its Validation, Technical Report 75, ECMWF, Reading, UK, 1995.

Viterbo, P. and Betts, A.: Impact on ECMWF Forecasts of Changes to the Albedo of the Boreal Forests in the Presence of Snow, Journal of Geophysical Research, 104, 27 803–27 810, 1999.

World Meteorological Organization: Guidelines on Ensemble Prediction Systems and Forecasting, Tech. Rep. WMO-No. 1091, World Meteorological Organization, Geneva, Switzerland, 2012.

Wu, X., Nan, Z., Zhao, S., Zhao, L., and Cheng, G.: Spatial Modeling of Permafrost Distribution and Properties on the Qinghai-Tibet Plateau, Permafrost and Periglacial Processes, 29, 86–99, https://doi.org/10.1002/ppp.1971, 2018.

Xia, Y., Ek, M., Sheffield, J., Livneh, B., Huang, M., Wei, H., Feng, S., Luo, L., Meng, J., and Wood, E.: Validation of Noah-Simulated Soil Temperature in the North American Land Data Assimilation System Phase 2, Journal of Applied Meteorology and Climatology, 52, 455–471, https://doi.org/10.1175/JAMC-D-12-033.1, 2013.

Xiao, Y., Zhao, L., Dai, Y., Li, R., Pang, Q., and Yao, J.: Representing Permafrost Properties in CoLM for the Qinghai-Xizang (Tibetan) Plateau, Cold Regions Science and Technology, 87, 68–77, 2013.

Xie, P., Chen, M., Yang, S., Yatagai, A., Hayasaka, T., Fukushima, Y., and Liu, C.: A Gauge-Based Analysis of Daily Precipitation over East Asia, Journal of Hydrometeorology, 8, 607 – 626, https://doi.org/10.1175/JHM583.1, 2007.

Xu, W., Sun, C., Zuo, J., Ma, Z., Li, W., and Yang, S.: Homogenization of Monthly Ground Surface Temperature in China during 1961–2016 and Performances of GLDAS Reanalysis Products, Journal of Climate, 32, 1121–1135, https://doi.org/10.1175/JCLI-D-18-0275.1, 2019.

Xue, Y., Huang, B., Hu, Z.-Z., Kumar, A., Wen, C., Behringer, D., and Nadiga, S.: An Assessment of Oceanic Variability in the NCEP Climate Forecast System Reanalysis, Climate Dynamics, 37, 2511–2539, https://doi.org/10.1007/s00382-010-0954-4, 2011.

Yang, K. and Zhang, J.: Evaluation of Reanalysis Datasets against Observational Soil Temperature Data over China, Climate Dynamics, 50, 317–337, https://doi.org/10.1007/s00382-017-3610-4, 2018.

Yang, S., Li, R., Wu, T., Hu, G., Xiao, Y., Du, Y., Zhu, X., Ni, J., Ma, J., Zhang, Y., Shi, J., and Qiao, Y.: Evaluation of Reanalysis Soil Temperature and Soil Moisture Products in Permafrost Regions on the Qinghai-Tibetan Plateau, Geoderma, 377, 114 583, https://doi.org/10.1016/j.geoderma.2020.114583, 2020.

Yi, Y., Kimball, J. S., Chen, R. H., Moghaddam, M., and Miller, C. E.: Sensitivity of Active-Layer Freezing Process to Snow Cover in Arctic Alaska, The Cryosphere, 13, 197–218, https://doi.org/10.5194/tc-13-197-2019, 2019.

Yukon Geological Survey: Yukon Permafrost Reports Data. In: Yukon Permafrost Database. Government of Yukon, 2021.

Zhan, M.-j., Xia, L., Zhan, L., and Wang, Y.: Evaluation and Analysis of Soil Temperature Data over Poyang Lake Basin, China, Advances in Meteorology, 2020, 1–11, https://doi.org/10.1155/2020/8839111, 2020.

Zhang, J., Wang, W.-C., and Wei, J.: Assessing Land-Atmosphere Coupling Using Soil Moisture from the Global Land Data Assimilation System and Observational Precipitation, Journal of Geophysical Research: Atmospheres, 113, https://doi.org/10.1029/2008JD009807, https://doi.org/10.1029/2008JD009807, 2008.

Zhao, L., Cheng, G., Li, S., Zhao, X., and Wang, S.: Thawing and Freezing Processes of Active Layer in Wudaoliang Region of Tibetan Plateau, Chinese Science Bulletin, 45, 2181–2187, https://doi.org/10.1007/BF02886326, 2000.

Zhao, T., Guo, W., and Fu, C.: Calibrating and Evaluating Reanalysis Surface Temperature Error by Topographic Correction, Journal of Climate, 21, 1440–1446, 2008.